

Astrocytes Transplanted during Early Postnatal Development Integrate, Mature, and Survive Long Term in Mouse Cortex

Sabrina Chierzi,¹ J. Benjamin Kacerovsky,¹ Albert H. K. Fok,¹ Sylvie Lahaie,¹ Arielle Shibi Rosen,¹ W. Todd Farmer,¹ and Keith K. Murai^{1,2}

¹Centre for Research in Neuroscience, Department of Neurology and Neurosurgery, Brain Repair and Integrative Neuroscience Program, Research Institute of the McGill University Health Centre, Montreal General Hospital, Montreal, Quebec H3G 1A4, Canada and ²Quantitative Life Sciences Graduate Program, McGill University, Montreal, Quebec H3A 2A7, Canada

Astrocytes have complex structural, molecular, and physiological properties and form specialized microenvironments that support circuit-specific functions in the CNS. To better understand how astrocytes acquire their unique features, we transplanted immature mouse cortical astrocytes into the developing cortex of male and female mice and assessed their integration, maturation, and survival. Within days, transplanted astrocytes developed morphologies and acquired territories and tiling behavior typical of cortical astrocytes. At 35–47 d post-transplantation, astrocytes appeared morphologically mature and expressed levels of EAAT2/GLT1 similar to nontransplanted astrocytes. Transplanted astrocytes also supported excitatory/inhibitory (E/I) presynaptic terminals within their territories, and displayed normal Ca^{2+} events. Transplanted astrocytes showed initially reduced expression of aquaporin 4 (AQP4) at endfeet and elevated expression of EAAT1/GLAST, with both proteins showing normalized expression by 110 d and one year post-transplantation, respectively. To understand how specific brain regions support astrocytic integration and maturation, we transplanted cortical astrocytes into the developing cerebellum. Cortical astrocytes interlaced with Bergmann glia (BG) in the cerebellar molecular layer to establish discrete territories. However, transplanted astrocytes retained many cortical astrocytic features including higher levels of EAAT2/GLT1, lower levels of EAAT1/GLAST, and the absence of expression of the AMPAR subunit GluA1. Collectively, our findings demonstrate that immature cortical astrocytes integrate, mature, and survive (more than one year) following transplantation and retain cortical astrocytic properties. Astrocytic transplantation can be useful for investigating cell-autonomous (intrinsic) and non-cell-autonomous (environmental) mechanisms contributing to astrocytic development/diversity, and for determining the optimal timing for transplanting astrocytes for cellular delivery or replacement in regenerative medicine.

Key words: astrocytes; confocal imaging; cortex; diversity; transplantation

Significance Statement

The mechanisms that enable astrocytes to acquire diverse molecular and structural properties remain to be better understood. In this study, we systematically analyzed the properties of cortical astrocytes following their transplantation to the early postnatal brain. We found that immature cortical astrocytes transplanted into cerebral cortex during early postnatal mouse development integrate and establish normal astrocytic properties, and show long-term survival *in vivo* (more than one year). In contrast, transplanted cortical astrocytes display reduced or altered ability to integrate into the more mature cerebral cortex or developing cerebellum, respectively. This study demonstrates the developmental potential of transplanted cortical astrocytes and provides an approach to tease apart cell-autonomous (intrinsic) and non-cell-autonomous (environmental) mechanisms that determine the structural, molecular, and physiological phenotype of astrocytes.

Received Mar. 16, 2022; revised Dec. 15, 2022; accepted Jan. 6, 2023.

Author contributions: S.C., W.T.F., and K.K.M. designed research; S.C., J.B.K., A.H.K.F., S.L., and A.S.R. performed research; S.C., J.B.K., A.H.K.F., S.L., A.S.R., W.T.F., and K.K.M. analyzed data; S.C. and K.K.M. wrote the first draft of the paper; S.C., W.T.F., and K.K.M. edited the paper; S.C. and K.K.M. wrote the paper.

This work was supported by Canadian Institutes of Health Research Grants PJT148569 and 156247 (to K.K.M.), Natural Sciences and Engineering Research Council of Canada Grants 408044-2011 and 69404 (to K.K.M.), and a Joint Canada-Israel Research Program Award provided by the International

Development Research Center (IDRC)/Israel Science Foundation/Canadian Institutes of Health Research/Azrieli Foundation.

The authors declare no competing financial interests.

Correspondence should be addressed to Keith K. Murai at keith.murai@mcgill.ca.

<https://doi.org/10.1523/JNEUROSCI.0544-22.2023>

Copyright © 2023 the authors

Introduction

Astrocytes are non-neuronal cells of the CNS that have complex structural, molecular, and physiological properties enabling them to regulate ion homeostasis, neurotransmitter levels, synaptic function/plasticity, and brain energetics. They participate in key processes including breathing, feeding behavior, vision, olfaction, and sleep (Petzold et al., 2008; Schummers et al., 2008; Gourine et al., 2010; Kim et al., 2014; Clasadonte et al., 2017). Structurally, astrocytes in the gray matter occupy nonoverlapping territories and have complex morphologies comprised of myriad microscopic branches that interact with neurons, synapses, and other glial cell types (Salmon et al., 2021). Astrocytes also have specialized subcompartments including endfeet that contribute to neurovascular coupling and blood-brain-barrier maintenance (Chow and Gu, 2015). Probing the transcriptome of astrocytes demonstrates their unique molecular profile with channels, transporters, and other receptors/signaling molecules needed to regulate brain physiology and homeostasis (Cahoy et al., 2008; Y. Zhang et al., 2016). This transcriptome is altered in aging and CNS injury/disease, where some astrocytes acquire a reactive state that can be reparative or further damaging (Boisvert et al., 2018; Escartin et al., 2021).

How do astrocytes perform such complex and specific roles in the brain? An emerging concept is that diverse populations of astrocytes establish unique microenvironments around neurons to support brain circuit-specific functions (Khakh and Deneen, 2019). It is now understood that a combination of intrinsic and extrinsic factors contributes to astrocyte diversity. Transcription factor coding during astrocytic development contributes to the early establishment of region-specific astrocytic subtypes in the CNS, such as those in the spinal cord and cortex (Hochstim et al., 2008; Tsai et al., 2012). Studies have shown that astrocytes in distinct brain regions display differences in gene expression and functional properties. Single-cell mRNA profiling and transcriptomic mapping has differentiated astrocytic molecular profiles in the rodent cortex, indicating variability in astrocytic gene expression even within a specific brain region (Batiuk et al., 2020; Bayraktar et al., 2020). This is consistent with layer-specific structural/molecular adaptations of astrocytes (Lanjakornsiripan et al., 2018). Despite the growing knowledge of astrocytic diversity in the CNS, the cell-autonomous and non-cell-autonomous mechanisms that stratify their properties remain to be better understood (Ben Haim and Rowitch, 2017). Understanding these processes is important in revealing how astrocytes contribute to brain microenvironments and circuit function, and how they respond to CNS injury/disease (Sofroniew and Vinters, 2010; Escartin et al., 2021).

In this study, we use an astrocyte transplantation approach to understand how immature cortical astrocytes integrate, mature, and survive in the brain. Previous studies have demonstrated the utility of cell transplantation to investigate the ability of neural or glial-restricted precursor cells to produce astrocytes and functionally integrate into the adult brain (Emmett et al., 1991; Ben Menachem-Zidon et al., 2011; K. Zhang et al., 2016) and to investigate the role of astrocytes in promoting brain plasticity and regeneration following injury (Smith and Miller, 1991; Müller and Best, 1989; Filous et al., 2010). Cellular grafting to the immature brain has also been used to study migration patterns of astrocytes (Zhou and Lund, 1992; Hatton et al., 1993). However, there remains a significant gap in our understanding of the structural, molecular, and physiological properties of astrocytes following their transplantation. Here, we provide a detailed characterization

of astrocytes following their transplantation into the cortex of early postnatal mice. We found that these cells successfully establish structural, molecular, and physiological features of protoplasmic astrocytes. In contrast, immature astrocytes transplanted into more mature cortex can survive, but mostly stay close to the transplantation site and have heterogenous properties with some astrocytes appearing reactive. Interestingly, immature cortical astrocytes transplanted into the developing cerebellar cortex can mature and establish unique spatial territories, but retain structural/molecular features of cortical astrocytes. Our findings demonstrate that astrocytes transplanted to the immature brain mimic astrocytes in recipient mice, and indicate that astrocytic transplantation can be useful for investigating cell-intrinsic and environmental mechanisms contributing to astrocytic development and function.

Materials and Methods

Animals

Experiments were done according to policies set forth by the Canadian Council on Animal Care and the Montreal General Hospital Facility Animal Care Committee. Mice were maintained in standard housing conditions and with continuous access to food and water. Both male and female mice were used for experiments. Astrocytic cultures were prepared from *Aldh1l1*-Tom mice, which contain an inducible Cre allele driven by the astrocyte-specific aldehyde dehydrogenase family 1, member L1 (*Aldh1l1*) promoter (*Aldh1l1*-CreERT2; The Jackson Laboratory; Srinivasan et al., 2016) and the floxed-stop Tomato allele (Madisen et al., 2010; Ai9; The Jackson Laboratory). C57BL/6 mice or *Aldh1l1*-eGFP-Stop-DTA BAC (*Aldh1l1*-eGFP) mice were used as transplant recipients (Tsai et al., 2012; The Jackson Laboratory). In some experiments, recombination of the floxed-stop Tomato allele was induced before culture preparation by injecting *Aldh1l1*-Tom pups with tamoxifen (Sigma). We used either of the following tamoxifen administration regimens: (1) 25 mg/kg tamoxifen for two consecutive days starting at P0–P1 or (2) 75 mg/kg tamoxifen for two to three consecutive days starting at P3 (Ishii et al., 2021).

Astrocytic cultures

Astrocytic cultures were prepared from P4–P8 mice following a method adapted from Chouchane and Costa (Chouchane and Costa, 2018). Cerebral cortices or cerebella were dissected in cold HBSS and meninges removed. Brain tissue was triturated using a 1000- μ l pipette into 1- to 2-mm tissue fragments in an Eppendorf tube containing HBSS with Ca^{2+} and Mg^{2+} . HBSS was decanted leaving behind tissue fragments that were then transferred to T75 flasks (Sarstedt) containing culture medium [F12-DMEM (Invitrogen) supplemented with 10% fetal bovine serum (Invitrogen), 5% horse serum (Invitrogen), 1% penicillin/streptomycin (Invitrogen), 20 ng/ml EGF (Genscript, Invitrogen), 20 ng/ml FGF2 (Invitrogen)] and placed at 37°C, 5% CO_2 . After tissue fragments adhered to the bottom of the flask (now referred to as explants), the explants were thoroughly washed with PBS to remove cellular debris and concentrate the number of astrocytes by reducing microglia, oligodendrocytes, and neurons before incubation in culture medium. Astrocytic cultures were maintained at 37°C, 5% CO_2 for 14–34 d before collection for transplantation. This allowed sufficient time for astrocytes to migrate away from the explants. For one experiment we used a batch of astrocytes that had been frozen and thawed but did not show any differences in properties from other batches of astrocytes. Cultures were passaged on reaching cell confluency. (z)-4-hydroxytamoxifen (tamoxifen, 2 μ g/ml, Millipore Sigma, Tocris) was added to the culture medium at least 2 d before transplantation to induce *Aldh1l1*-driven Tomato expression. Before transplantation, astrocytes were dissociated with trypsin/EDTA (Invitrogen), washed twice in HBSS with Ca^{2+} and Mg^{2+} and re-suspended in HBSS at a density of 40,000–100,000 cells/ μ l.

Immunofluorescence of cultured cells

Trypsin-dissociated cells from tamoxifen-treated astrocyte cultures were seeded on poly-D-lysine-coated coverslips (0.1 mg/ml), maintained in

supplemented culture medium (see above, Astrocytic Cultures) and fixed in 4% paraformaldehyde/0.1 M phosphate buffer (PFA) a few days later. After being rinsed in PBS (Invitrogen), and kept in blocking solution [5% normal donkey serum (NDS; Jackson ImmunoResearch), 0.2% Triton X-100 (Sigma) in PBS] for 20–30 min, cells were incubated with primary antibodies for 1 h at room temperature (RT). The following antibodies were used: anti-Sox9, 1:300 (rabbit polyclonal; Millipore); anti-Sox9, 1:300 (goat polyclonal; Novus); anti-NG2, 1:300 (rabbit polyclonal; Millipore); anti-Olig2, 1:250 (rabbit polyclonal; EMD Millipore); anti-GFAP, 1:500 (rabbit polyclonal; EMD Millipore); anti-GFAP, 1:300 (mouse monoclonal; Invitrogen); and anti-Kir4.1, 1:500 (guinea pig polyclonal; Alomone Labs). After washing in PBS, cells were incubated with secondary antibodies conjugated with Alexa or DyLight fluorophores (1:500, Invitrogen, Jackson ImmunoResearch) for 30 min to 1 h at RT. DAPI was also applied to visualize cells nuclei. Coverlips were mounted on slides with SlowFade Gold (Life Technologies) before imaging.

Cell transplantation

Cells were transplanted to cerebral or cerebellar cortices between postnatal P3 and P8 (P3–P8). Pups were anesthetized using hypothermia by placing them on crushed ice until cessation of movements and reflexes, and kept on a cold gel pack for the duration of the procedure. A cellular suspension (1 μ l) containing astrocytes was injected unilaterally into the cortex at a speed of 0.5–1 μ l/min using a pulled glass pipette (Warner Instruments, 100- μ m internal diameter) attached to a Hamilton syringe. Injections were performed directly through the skin and soft skull at a depth of 0.7–1.2 mm from the skin with an injection controller (Harvard Apparatus). For injections into the cerebellum, anesthetized pups were placed on cold gel packs with their head slightly tilted forward to make the cerebellum more accessible to the glass needle. After cell transplantation, mice were warmed on a heating pad or under an infrared lamp. Pups were then gently rubbed with cage bedding to mask procedure-related scents that may prevent maternal care before being returned to the dam.

For cell transplantation procedures between postnatal days 34 and 43, mice were anesthetized with isoflurane and mounted onto a stereotaxic frame. A longitudinal incision through the skin (1 cm) was performed to expose the skull, and a small hole (diameter roughly 1 mm) was drilled through the bone with a microsurgical drill (Ideal Micro Drill, Harvard Apparatus). The dural membrane was pierced with sharp forceps or insulin syringe needle, and the cell suspension was injected into the cortex as described above at a depth ranging from 0.3 to 0.7 mm from the brain surface. The skin near the injection site was sutured closed and mice were returned to their cages following their recovery from anesthesia. Analgesia was provided according to standard operating procedures at the Animal Resources Division of the Research Institute of the McGill University Health Center.

Immunofluorescence of brain sections

Mice were transcardially perfused with 4% paraformaldehyde/0.1 M phosphate buffer (PFA) at different time points following transplantation (1 d, 3 d, 7 d, 35–47 d, 110–130 d, and 368–570 d). Brains were postfixed for 12–24 h in PFA, equilibrated in 30% sucrose-PBS, and frozen in optimal cutting temperature (OCT) compound (Sakura); 40- μ m sections were produced by a cryostat and immunolabeling was performed using a free-floating approach. After a 40 min to 2-h incubation in blocking solution [5% normal donkey serum (NDS; Jackson ImmunoResearch), 1% Triton X-100 (Sigma) in PBS], sections were incubated with primary antibodies. All antibody incubations were performed in 1% NDS, 0.2% Triton X-100 PBS. Washes were performed in blocking solution or in PBS. Most primary antibodies were applied for 3–5 h at room temperature or for 15–24 h at 4°C. Antibodies to excitatory amino acid transporters, vesicular glutamate transporters and vesicular GABA transporters were incubated for 48–72 h at 4°C to allow better antibody penetration and more uniform labeling throughout the tissue section. After washing, secondary antibodies conjugated with Alexa or DyLight fluorophores (1:500, Invitrogen, Jackson ImmunoResearch) were applied for 1–2 h at RT. The following primary antibodies were used: anti-green fluorescent protein (GFP), 1:500 (chicken polyclonal; Abcam); anti-glutamine synthetase (GS), 1:300 (mouse monoclonal; Millipore); anti-Sox9, 1:300 (rabbit polyclonal;

Millipore); anti-Sox9, 1:300 (goat polyclonal; Novus); anti-NG2, 1:300 (rabbit polyclonal; Millipore); anti-excitatory amino acid transporter 1 (EAAT1/GLAST), 1:500 (rabbit polyclonal; Abcam, Synaptic Systems); anti-excitatory amino acid transporter 2 (EAAT2/GLT1), 1:500 (guinea pig polyclonal; Millipore); anti-aquaporin 4 (AQP4), 1:500 (rabbit polyclonal; Alomone Labs); anti-gial fibrillary acidic protein (GFAP), 1:500 (guinea pig polyclonal; Synaptic Systems); anti-GFAP, 1:500 (rabbit polyclonal; Millipore); anti-vesicular glutamate transporter 1 (vGLUT1), 1:300 (guinea pig polyclonal; Millipore); anti-vesicular glutamate transporter 2 (vGLUT2), 1:300 (guinea pig polyclonal; Millipore); anti-vesicular GABA transporter (VGAT), 1:500 (rabbit polyclonal; Synaptic Systems); anti-GluA1, 1:500 (rabbit polyclonal; Millipore); anti-Calbindin, 1:500 (rabbit polyclonal; Synaptic Systems); anti-Calbindin, 1:500 (guinea pig polyclonal; Synaptic Systems); anti-Connexin 30, 1:200 (rabbit polyclonal; Invitrogen); anti-Connexin 43, 1:300 (mouse monoclonal; BD Biosciences); anti-Type IV Collagen, 1:250 (goat polyclonal; Southern Biotech); anti-Olig2, 1:250 (rabbit polyclonal; EMD Millipore); anti-Ki67, 1:300 (rabbit polyclonal; Abcam); anti-Necab1, 1:200 (rabbit polyclonal; Atlas Antibodies); anti-Kir4.1, 1:500 (guinea pig polyclonal; Alomone Labs); anti-active caspase 3, 1:250 (rabbit polyclonal; Cell Signaling). Tissue sections were mounted onto slides and coverslipped using SlowFade Gold (Life Technologies) before imaging.

Image acquisition and analysis

Microscopy

Images were acquired using a laser scanning confocal microscope and Fluoview image-acquisition software (Olympus). The following objectives were used: 20 \times [numerical aperture (NA) = 0.85], 40 \times (NA = 1.3), 60 \times (NA = 1.4).

Characterization of cultured cells

To understand the cellular identity of Tomato+ cells before transplantation, we performed immunolabeling for Sox9 and NG2 to detect astrocytes and oligodendrocyte precursors, respectively. Single plane images of fixed cells were acquired for the Tomato, Sox9, and NG2 signals. Tomato+ cells were classified as either astrocytes (Sox9+), astrocyte intermediates (Sox9+/NG2+), oligodendrocyte precursors (NG2+), or “other” (negative for either marker). We counted a total of 233–367 cells from each of three different batches of cultured cells (number of cells per batch: 233, 242, 367) and estimated their distribution into the classes mentioned above. In a parallel analysis, we labeled fixed cells for Sox9 and for the glial progenitor marker Olig2 (Marshall et al., 2005; Clavreul et al., 2019), and classified Tomato+ cells in four classes, namely, “Sox9+,” “Sox9+/Olig2+,” “Olig2+,” and “Sox9–/Olig2–” (also rereferred to as “Other”), according to the expression of either marker. We counted a total of 170–529 cells from each of four different batches of cells (number of cells per batch: 295, 529, 302, 170).

To assess astrocyte heterogeneity in our cultures, we immunolabeled four different astrocyte batches for GFAP and the potassium channel Kir4.1 and measured signal intensities for both markers using CellProfiler 4.2.1 (Stirling et al., 2021). The cytoplasmic Tomato signal was used as a mask to identify individual cells and their respective morphologies. The intensities of GFAP and Kir4.1 were measured for every identified cell that was not touching the boundaries of the image. Cells containing a Sox9+ nucleus within their borders were classified as astrocytes. The measured mean intensities of GFAP and Kir4.1 of individual astrocytes (number of astrocytes per batch: 383, 608, 402, 286) were correlated using the correlation function in R. The complete details of the Cell Profiler pipeline and the R code used to parse the resulting data can be found at <https://github.com/murailab>.

Characterization of transplanted cells during development

Image stacks were acquired (z step = 3 μ m) from sections of transplanted brains immunolabeled for Sox9 and NG2. For each mouse, we counted a total of 33–272 Tomato+ cells and classified them as either astrocytes, oligodendrocyte precursors, or “other” (see above, Characterization of cultured cells). The following numbers of mice

and cells were included in each experimental group: 7 d post-transplantation (DPT), four mice, 474 cells; 35–47 DPT, three mice, 407 cells; 110–130 DPT, five mice, 880 cells; 368 DPT, three mice, 272 cells. To estimate the amount of glial progenitors among transplanted astrocytes, we performed immunolabeling for Sox9 and for the glial progenitor marker Olig2 on brain sections collected at 1 DPT and 3 DPT. We counted the number of Olig2+ nuclei and Sox9+ nuclei among Tomato+ cells on single-plane images, and calculated the average fraction of Olig2+/Sox9+ cells in transplanted astrocytes per mouse and per experimental group. A total of 731 cells (three mice) and 646 cells (three mice) were counted in this quantification for the 1 DPT and 3 DPT group, respectively. Similarly, to quantify the fraction of transplanted astrocytes undergoing cell-proliferation at different times after transplantation, we performed immunolabeling for the cell-proliferation marker Ki67 and calculated the fraction of Ki67+/Sox9+ nuclei in transplanted astrocytes. The following numbers of mice and cells were included in each experimental group: 1 DPT, four mice, 1078 cells; 3 DPT, four mice, 730 cells; 7 DPT, three mice, 471 cells; 35–47 DPT, three mice, 471 cells.

Quantification of the number of transplanted astrocytes

To assess the survival of transplanted astrocytes at different times after transplantation, we quantified the average number of Tomato+ astrocytes per section at 7 DPT and 368–570 (368+) DPT. We acquired 12- μ m-deep image-stacks from brain sections labeled for Sox9, and counted the total number Sox9+/Tomato+ cells per section, keeping cells aligned along the pial membrane (pial astrocytes) and parenchymal astrocytes in two distinct groups. We analyzed three sections from each of three mice at 7 DPT and three to four sections from each of three mice at 368+ DPT. We then calculated the average number of transplanted astrocytes per mouse (astrocytes/section/mouse), and the average number of transplanted astrocytes/section for each experimental group across mice. We also used this cell counting analysis to estimate the average fraction of transplanted astrocytes that localize along the pial membrane at 7 DPT and 368+ DPT (excluding cells located along the track of the injection site).

Astrocyte migration analysis

To estimate the migration of transplanted astrocytes from the injection site we acquired low-resolution images (10 \times or 20 \times) from sections of transplanted brains collected at 7 and 110–130 DPT and quantified the lateral spread of parenchymal Tomato-positive astrocytes. We measured the maximum distance between transplanted astrocytes in the direction perpendicular to the injection track (in images containing the injection track) or along the medio-lateral axis (in images with no injection track) and defined this measurement as lateral migration distance (LMD). We estimated LMD values in mice transplanted at P3–P7 (developmental transplantation) across different times after transplantation, namely, 7 DPT, 35–47 DPT, and 110–130 DPT. Since mice in the 7 DPT group are P10–P14, an age at which the mouse brain is still increasing in size, it may be possible to detect lower distance between transplanted astrocytes in this group just because of lower cell displacement. To adjust for brain size differences between time points which could affect lateral migration distance calculation, we multiplied LMD values measured at 7 DPT by 1.07, that represents the linear scale factor between brains at 7 DPT and later time points. We then calculated the mean LMD value per mouse and the mean LMD value for each experimental group. The following numbers of mice and sections were used for each experimental group: 7 DPT, five mice, 30 sections; 35–47 DPT, five mice, 17 sections; 110–130 DPT, nine mice, 45 sections. In some cases, it was difficult to clearly observe the injection site based on Tomato signal only.

To evaluate whether the age of the mice receiving astrocyte transplantation affects the migration of transplanted astrocytes from the injection site, we compared LMD values at 35–47 DPT between mice transplanted at P3–P7 (P7) and mice transplanted at P34–43 (P34), using the same method described above. Since the brain size was equivalent in the two experimental groups, we did not apply any scale factor. The numbers of mice/sections used for this analysis were five mice, 17

sections for the transplantation at P7, and five mice and 20 sections for the transplantation at P34.

Analysis of astrocyte distribution across layers

To quantify the distribution of astrocytes across cortical layers at 35–47 DPT, we identified cortical layering using anatomic measures (i.e., relatively cell-free composition of layer 1) and immunolabeling for Necab1, a neuronal marker diffusely expressed by layer 4 neurons. The faint and nonspecific labeling of neurons with the Sox9 antibody also allowed us to identify neurons in layers 2–6. We assessed the distribution of transplanted astrocytes (Sox9+/Tomato+ cells) in these regions for five mice and calculated the average distribution across mice. We used 104–374 cells for each of the five different mice (282, 269, 374, 360, 104), excluding from the analysis astrocytes aligned along the pial surface which could not be individually identified.

Astrocytic tiling

To investigate whether transplanted astrocytes occupy discrete territories in the cortex (“tiling”), we analyzed brain sections from Aldh111-eGFP mice transplanted with Tomato+ astrocytes. Since nontransplanted astrocytes in Aldh111-eGFP mice express GFP, the extent of overlap between transplanted (Tomato+) and nontransplanted (GFP+) astrocytes was measured by determining the colocalization of Tomato and GFP signals. In single-plane confocal images, rectangular ROIs were chosen from image fields that contained territories from Tomato+ and GFP+ astrocytes taking up approximately the same area. The JACoP (Just Another Colocalization Plugin) ImageJ plugin was used to assess colocalization in each ROI. This plugin converts thresholded GFP and Tomato images into binary images, and returns the Manders’ coefficients M1 and M2. M1 is defined as the ratio of the colocalized GFP-Tomato pixel intensity to the total GFP pixel intensity and indicates the fraction of GFP colocalizing with Tomato. M2 is defined as the ratio of the colocalized GFP-Tomato pixel intensity to the total Tomato pixel intensity and indicates the fraction of Tomato colocalized with GFP. Manders’ coefficients of 0 and 1 indicate zero and full colocalization, respectively. To provide a positive control for colocalization, we also calculated the Manders’ coefficients representing the overlap between Tomato and the astrocyte marker glutamine synthetase (GS). Both proteins are located in the astrocytic cytoplasm.

M1 and M2 Manders’ coefficients were calculated at 35–47 DPT. A total of 42 fields (three mice) were used to assess colocalization between Tomato and GFP signals, while 25 fields (three mice) were used for colocalization between Tomato and GS signals. The coefficient value for each field, the mean coefficient value for each mouse, as well as total mean value across all mice were calculated.

To assess whether the exclusive cortical territories occupied by astrocytes in the transplanted cortex have similar or smaller size compared with those occupied by astrocytes in the nontransplanted cortex, we compared astrocyte density between the transplanted cortex and the contralateral one. We performed Sox9 immunolabeling on sections collected from transplanted mice at 35–47 DPT and estimated the density of Sox9+ cells from single-plane images. Since we observed that the majority of transplanted astrocytes were confined in layers 1–3 of the cortex, we restricted our analysis to these layers. We analyzed three sections from each of four mice and estimated the ratio of Sox9+ cell density between transplanted and contralateral cortex for each section and the average ratio per mouse across sections.

Astrocyte marker expression

The expression levels of the glutamate transporters EAAT2/GLT1, EAAT1/GLAST, the cytoskeleton protein glial fibrillary acidic protein (GFAP), and the water channel aquaporin 4 (AQP4) were compared between transplanted astrocytes and nontransplanted astrocytes. Single-plane images were acquired with the 60 \times objective from sections labeled for the markers above. For transplantation experiments performed in Aldh111-eGFP mice, nontransplanted astrocytes from the recipient mouse were identified based on GFP expression and absence of Tomato. For experiments performed in C57BL/6 mice, nontransplanted astrocytes were identified by their labeling for GS and

absence of Tomato. In each image, ROIs were drawn to define territories covered by transplanted and nontransplanted astrocytes. ROIs selected for nontransplanted astrocytes were chosen to closely match the shape, size, and cortical depth of the ROI selected for transplanted astrocytes. For EAAT1/GLAST and EAAT2/GLT1 quantifications, only astrocytic processes were included in the ROIs and the cell bodies were excluded. For GFAP quantifications, both cell bodies and processes were included. Since AQP4 is highly concentrated at astrocytic endfeet, AQP4 expression was specifically quantified in this compartment. Image fields were chosen where transplanted and nontransplanted astrocytes contacted the same blood vessel. Mean intensity values for each marker (average gray values) were quantified within each ROI using ImageJ. A transplanted/nontransplanted ratio for each marker was defined as the intensity measured for the transplanted astrocyte over the one measured for the nontransplanted astrocyte.

The following number of fields and mice were included in each experimental group: GFAP-110 DPT, four mice, 96 fields; EAAT2/GLT1-35 DPT, five mice, 61 fields; EAAT2/GLT1-110 DPT, nine mice, 93 fields; EAAT1/GLAST-35 DPT, five mice, 58 fields; EAAT1/GLAST-110 DPT, nine mice, 88 fields; EAAT1/GLAST-368+ DPT, seven mice, 66 fields; AQP4-35 DPT, five mice, 80 fields; AQP4-110 DPT, eight mice, 77 fields. Ratio values of marker intensity were calculated between transplanted and nontransplanted astrocytes for each image, for each mouse, and across all mice in the same experimental group. In a parallel set of experiments, we performed EAAT2/GLT1 and EAAT1/GLAST quantification in mice transplanted at P34–P43 and collected at 110–130 DPT. Eight to 10 image fields from each of four mice were used (number of fields per mouse: 10, 9, 10, 8).

Density of presynaptic terminals in astrocytic territories

Single-plane images were acquired with a 60× objective from tissue sections labeled for the excitatory presynaptic proteins vesicular glutamate transporter 1/2 (vGLUT1/2) or inhibitory presynaptic protein vesicular GABA transporter (VGAT). ROIs representing territories covered by transplanted and nontransplanted astrocytes were identified, according to the criteria described above for the quantification of EAAT1/GLAST and EAAT2/GLT1 expression. A custom-made ImageJ macro was used to measure the cumulative surface covered by presynaptic terminals in the selected ROIs. vGLUT1/2 and VGAT image channels were converted into binary images, and the cumulative area of particles with a surface larger than 0.05 μm^2 was calculated in each ROI. Particle coverage, defined as the particle cumulative area divided by the ROI area, was calculated for both transplanted and nontransplanted astrocyte territories. The ratio of particle coverage in transplanted astrocytes versus particle coverage in nontransplanted astrocytes was computed for every image. The following number of fields and mice were included in each experimental group: vGLUT1/2-110 DPT, six mice, 59 fields; VGAT-110 DPT, six mice, 76 fields.

Astrocyte heterogeneity analysis

In brain sections collected at 35–47 DPT, we used immunolabeling for Sox9 and for the neuronal marker Necab1 to identify four layer regions (layer 1, layers 2–3, layer 4, and layers 5–6; see above, Analysis of astrocyte distribution across layers). We also labeled these sections for either GFAP or the potassium channel Kir4.1 and acquired single-plane 20× images for all four signals (Sox9, Necab1, Tomato and GFAP/Kir4.1). ROIs were identified in layer 1 and layers 2–3 for transplanted (Sox9+/Tomato+) and nontransplanted (Sox9+/Tomato-) astrocytes, and the mean intensity value for either Kir4.1 and GFAP was calculated in each ROI. We avoided regions of layer 1 too close to the pial membrane, as we often observed a sudden increase in the intensity of both GFAP/Kir4.1 signals close to the brain surface, possibly reflective of astrocyte reactivity. For each section we acquired ROIs related to four different groups of astrocytes, namely, transplanted-layer 1 (T1), transplanted-layers 2–3 (T2), nontransplanted-layer 1 (NT1), and nontransplanted-layers 2–3 (NT2). In each section and for each of the four astrocyte groups, we calculated the average value for either Kir4.1 or GFAP intensity across all ROIs (Kir4.1/GFAP intensity per section). We

then calculated the average Kir4.1/GFAP intensity values per mouse across all sections and compared average values per mouse between the two layer regions. The following numbers of mice and sections were used for this analysis: Kir4.1-T1, six mice, 15 sections; Kir4.1-T2, six mice, 16 sections; Kir4.1-NT1, six mice, 15 sections; Kir4.1-NT2, six mice, 16 sections; GFAP-T1, five mice, 15 sections; GFAP-T2, five mice, 14 sections; GFAP-NT1, five mice, 15 sections; GFAP-NT2, five mice, 14 sections.

Caspase 3 activation analysis

The amount of caspase 3 activation among transplanted astrocytes was compared at 1 DPT between two experimental groups, namely, mice transplanted at P3–P7 and mice transplanted at P34–P43. Brain sections were immunolabeled for active caspase 3 (Cas3) and single-plane images were acquired for Cas3 and Tomato signals. A custom-made ImageJ macro was used to measure the overlap between Cas3-positive particles and transplanted cells. For each image field, Cas3 and Tomato image channels were converted into binary images, and the cumulative area of Cas3 particles with a surface larger than 0.64 μm^2 and overlapping with Tomato signal was calculated. Cas3 coverage on Tomato+ cells was calculated by dividing the cumulative Cas3-Tomato overlap area by the total area covered by Tomato signal, and expressed as percentage. Average values of Cas3 coverage were calculated for each mouse across image fields, and for each experimental group across mice. The following number of mice/image fields were used: P3–P7, five mice, 48 image fields; P34–P43, three mice, 30 image fields.

Ca²⁺ imaging

Forty-seven days post-transplantation, mice were deeply anaesthetized with isoflurane and perfused through the right ventricle with 10 ml ice cold cutting solution (87 mM NaCl, 25 mM NaHCO₃, 2.5 mM KCl, 1.25 mM NaH₂PO₄, 25 mM D-glucose, 75 mM sucrose, 7 mM MgCl₂, and 0.5 mM CaCl₂ saturated with 95% O₂ and 5% CO₂). Brains were then quickly dissected and coronal cortical slices (300 μm) were cut on a Leica VT1200S vibratome in ice cold cutting solution. Slices were incubated for at least 1 h in artificial CSF (aCSF; 126 mM NaCl, 2.5 mM KCl, 1.3 mM MgCl₂, 10 mM D-glucose, 2.4 mM CaCl₂, 1.24 mM NaH₂PO₄, and 26 mM NaHCO₃ saturated with 95% O₂ and 5% CO₂) initially heated to 34–36°C and then allowed to equilibrate to room temperature. Slices were subsequently transferred in aCSF containing 5–10 μM Fluo-4AM (Thermo Fisher Scientific) and 2.5 $\mu\text{g}/\text{ml}$ pluronic acid. After 1-h incubation with Fluo-4AM, slices were transferred to dye-free aCSF for at least 30 min before imaging. For imaging, slices were transferred into a chamber mounted on the stage of a laser scanning microscope and continuously perfused with room temperature artificial CSF. Fluo-4AM and Tomato signals were imaged using 488 nm and 543 nm lines respectively at a frame rate of 1 Hz. To correct for image drift, we computed the relative frame by frame shift using the fftshift function in MATLAB, based on the red channel. We then applied the opposite series of shifts to each frame and cropped the image to only include pixels that were in frame for the entire duration of imaging. Identical shifts were applied to both channels. To reduce noise, we applied the medfilt3 function to the time series stack, with the default 3-by-3-by-3 filter. To correct for uneven illumination in the slices we applied a Gaussian blur filter ($\sigma = 20$ pixels) to each frame and divided the frame by the filtered image. For analysis, we used AQuA (Wang et al., 2019) with empirically determined parameters to identify individual Ca²⁺ events. Territories of nontransplanted astrocytes were estimated based on their Fluo-4AM loading and Ca²⁺ activity in areas that displayed no Tomato signal ($n = 4$ transplanted astrocytes, and $n = 6$ nontransplanted astrocytes).

Statistical analysis

The data for each experimental group were displayed as means with SEM. For statistical analysis of marker expression levels and presynaptic particle coverage in each experimental group, we looked at the mean values of transplanted/nontransplanted ratios for each mouse and compared this population to an equivalent population of transplanted/nontransplanted ratios equal to 1. We used a nonparametric Wilcoxon rank-sum test to check whether the two populations were

significantly different. We used the same test to estimate differences in astrocyte density between transplanted and contralateral cortex, by comparing the mean values of transplanted/controlateral ratios per mouse to an equivalent population of transplanted/controlateral ratios equal to 1. One-way ANOVA was used for measurements performed at more than two time points after transplantation, i.e., quantification of astrocyte lateral migration and quantification of astrocyte proliferation (Ki67 expression). We used an unpaired Student's *t* test to compare two experimental groups in the following analyses: quantification of glial precursors among transplanted astrocytes (1 DPT vs 3 DPT), number of transplanted astrocytes per section (7 DPT vs 368+ DPT), fraction of transplanted astrocytes associated to the pial membrane (7 DPT vs 368+ DPT), caspase 3 activation among transplanted astrocytes (developmental vs adult transplantation), astrocyte lateral migration (developmental vs adult transplantation), AQUA-based analyses of Ca²⁺ events (transplanted vs nontransplanted astrocytes). We compared mean values per mouse for all the measurements mentioned above except those included in the AQUA-based analysis of calcium dynamics. For this analysis, we calculated the average value of calcium-dynamics measurements per cell across calcium events and compared the average values per cell between transplanted and nontransplanted cells. We used a paired Student's *t* test to compare Kir4.1 and GFAP intensity levels between layer 1 and layers 2–3. Mean Kir4.1/GFAP intensity values per mouse were used for this comparison.

The number of mice, cells, and image fields analyzed can be found in the individual Materials and Methods sections. *p*-values can be found in the figure legends.

Results

Transplanted immature cortical astrocytes integrate into the developing cortex, display complex morphologies, and survive for greater than one year *in vivo*

To investigate how cortical astrocytes integrate, mature, and survive in the developing and mature brain, we developed a transplantation approach allowing us to transplant astrocytes from genetically modified donor mice to recipient mice (Fig. 1A). We prepared immature cortical astrocytes from postnatal day 4 to 8 (P4–P8) mice containing a tamoxifen-inducible CreERT2 allele driven by the astrocyte-specific aldehyde dehydrogenase family 1, member L1 (Aldh1l1) promoter (Srinivasan et al., 2016) and a floxed-stop tandem-dimer Tomato allele (Madisen et al., 2010; Ai9, now referred to as Tomato; Fig. 1B). Before transplantation, astrocytes were cultured, passaged, and treated with tamoxifen to induce Tomato expression (Fig. 1C) and analyzed by immunolabeling and confocal microscopy (Fig. 1D,E). Since Aldh1l1-CreERT2 drives Cre-mediated recombination specifically in astrocytes (Srinivasan et al., 2016), we expected that the majority of Tomato-positive (Tom+) cells would express the astrocytic marker Sox9 following tamoxifen induction. Consistent with this, 97.6 ± 1.5% of Tomato+ cells were positive for the astrocytic protein Sox9 (Fig. 1E), indicating a high degree of specificity of Cre recombination in astrocytes. Importantly, however, 83.7 ± 0.7% of Sox9+ astrocytes expressed Tomato, indicating that Cre-mediated recombination in astrocytes was high, but not complete. Given the lineage relationships between astrocytes and oligodendrocyte precursors (OPCs) (Kirdajova et al., 2021), we also labeled for the proteoglycan NG2 to test for the presence of Sox9+/NG2+ intermediate astrocytes (Zhu et al., 2012; Zuo et al., 2018), and Sox9–/NG2+ OPCs. We found that a fraction of Tom+/Sox9+ cells were also NG2+ (11.16 ± 3.23%); however, only 1 ± 0.5% Tom+/Sox9– cells expressed NG2. The remaining fraction of Tom+ cells (1.5 ± 1%) were SOX9– and NG2– and presumably precursors that have not differentiated into Sox9-positive astrocytes. These findings indicated that the majority of cells in our cultures were astrocytes and expressed Tomato following Cre-mediated recombination.

Following *in vitro* analysis, astrocytes were then harvested and transplanted into the cortex of P3–P7 mice, a time point when astrocytes are actively proliferating and developing in cortex (Ge et al., 2012; Clavreul et al., 2019). The brains of recipient mice were subsequently recovered at different time points after transplantation and analyzed for their expression of known astrocytic proteins (Fig. 1F). Analysis of recipient brains at 7 d post-transplantation (DPT) revealed the presence of Tom+/Sox9+ astrocytes in the cortex (Fig. 1G). Transplanted astrocytes were found in multiple cortical layers and showed elaborated processes typical of developing astrocytes in the brain (Bushong et al., 2004). In addition, we encountered many Tom+/Sox9+ cells adjacent to the pial surface, likely representing transplanted astrocytes that escaped the injection site and attached to the pial surface (Figs. 1G, 2A). These represented 59.8 ± 4.41% (7 DPT) and 61.05 ± 3.39% [368–570 (368+) DPT] of transplanted astrocytes, excluding the astrocytes trapped at the injection site. Quantifying the distribution of parenchymal Sox9+ astrocytes in brains collected at 35–47 DPT, we found that most transplanted astrocytes (77.76%) were localized in layer 1. A smaller fraction of transplanted astrocytes was observed in deeper layers (~22%): layers 2–3 (10.04%), layer 4 (4.42%), and layers 5–6 (7.78%; Fig. 2B). At 35–47 DPT and 110–130 DPT, transplanted astrocytes were retained in the cortex, developed morphologic features characteristic of mature protoplasmic astrocytes, including formation of large, complex arbors (Fig. 1G) and specialized endfeet surrounding blood vessels (Fig. 1G, arrows), and found to have similar lateral migration distances as those found at 7 DPT (Fig. 2C,D) indicating that transplanted astrocytes mostly reach their final position in the cortex by 7 DPT. At 368 DPT, Tomato+ astrocytes were present and continued to maintain their complex morphologies and association with cerebrovasculature (Fig. 1G).

The majority of parenchymal Tomato+ cells encountered showed morphologic properties typical of protoplasmic astrocytes (Fig. 3A,B). However, on occasion, we detected cells that did not have astrocytic morphology, but instead resembled other types of glia including OPCs (Fig. 3C,D). To account for these cells, we quantified the percentage of Tomato+ cells that were either Sox9+ (astrocytes), NG2+ (OPCs), or Sox9–/NG2– (neither astrocytes or OPCs), across all time points (7, 35–47, 110–130, and 368 DPT). Cells found along the pial surface were excluded from this analysis as it was difficult to resolve individual cells. At all time points, Sox9+ astrocytes with highly ramified morphologies were the most abundant transplanted cell type detected (90.5 ± 4.9% at 7DPT; 90.8 ± 8.4% at 35–47 DPT; 79.5 ± 11.9% at 110–130 DPT; 77.4 ± 9.8% at 368 DPT) with OPCs comprising between 5.6% and 16.1% of transplanted cells (5.6 ± 3.2% at 7 DPT; 8.5 ± 7.7% at 35–47 DPT, 16.1 ± 9% at 110–130 DPT; 8.7 ± 3.8% at 368+ DPT; Fig. 3E). A small group of cells were neither Sox9+ nor NG2+ and often displayed a small round cell body and few thin processes, potentially representing more mature oligodendrocytes (Fig. 3D). These data showed that the vast majority of parenchymal Tomato+ transplanted cells were protoplasmic astrocytes.

Given our previous result showing a large proportion of immature astrocytes and a small proportion of OPCs in pretransplantation cultures (Fig. 1D,E), we further investigated the fate of transplanted cells following their transplantation. We first examined *in vitro* the degree of co-expression of Sox9 with Olig2, a marker of glial progenitors (Marshall et al., 2005; Clavreul et al., 2019) in pretransplantation cultures. We found that the majority of Tom+ cells (78.77 ± 2.21%) were positive for Sox9 and Olig2 (Fig. 3F,G), while only a small proportion

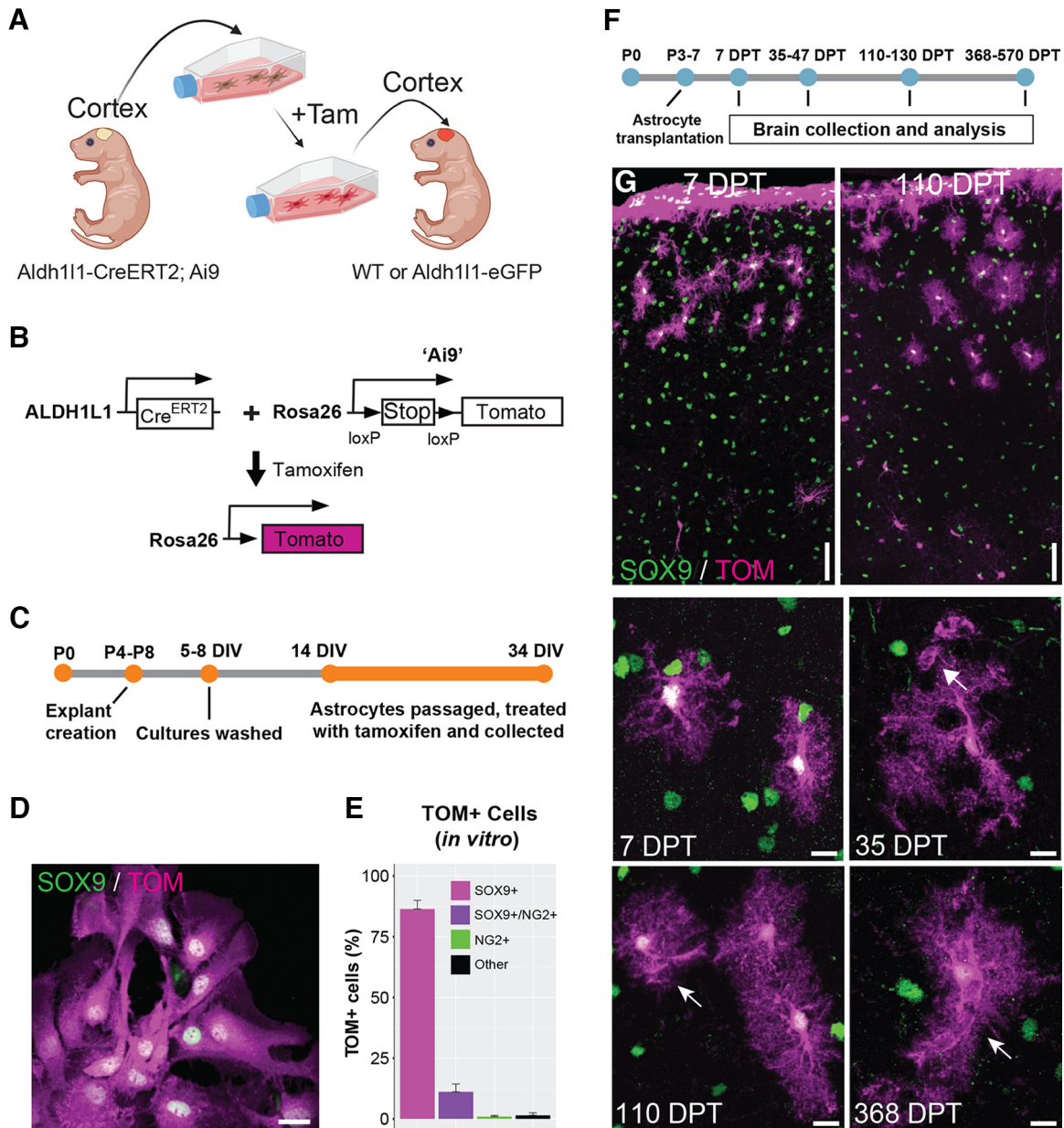


Figure 1. Cortical astrocytes transplanted into the immature cortex display protoplasmic astrocyte morphology starting within a few days after transplantation. **A**, Overview of the experimental design for transplantation of cortical astrocytes into the cerebral cortex of mouse pups. *Tam* = 4-hydroxytamoxifen. Figure created with BioRender. **B**, Schematic showing the genetic background of the mice used as transplant donors. *Tamoxifen* = 4-hydroxytamoxifen. **C**, Timeline of culture preparation. **D**, Cultured astrocytes expressing Tomato following tamoxifen administration. Tom = Tomato. **E**, Percentage of Tomato+ cells *in vitro* expressing Sox9 (astrocytes), Sox9 and NG2 (intermediate astrocytes), NG2 (OPCs), or neither marker (“Other”). **F**, Timeline of astrocyte transplantation. **G**, Transplanted astrocytes at different days post-transplantation (DPT). Transplanted cells are labeled with Tomato (TOM) and astrocytes are detected by SOX9 immunolabeling (green). Arrows indicate astrocyte endfeet. 35 DPT = 35–47 DPT, 110 DPT = 110–130 DPT. Scale bar: 20 μ m (**D**) and 50 and 10 μ m (**G**, top panels, and **G**, middle and bottom panels, respectively).

of cells were Olig2+ and Sox9– ($6.91 \pm 0.86\%$), indicating that most pretransplantation cells in culture are Olig2+ immature astrocytes. Interestingly, analysis *in vivo* found that only $22.73 \pm 1.37\%$ of transplanted astrocytes were Sox9+/Olig2+ at 1 DPT and that this proportion decreased to $5.6 \pm 0.7\%$ by 3 DPT (Fig. 3H,I), suggesting progressive astrocytic maturation during the first few days *in vivo* following transplantation. This maturation was consistent with the finding that transplanted cells at 1 DPT showed a fusiform, elongated morphology typical of migrating cells. However, by three DPT, most of transplanted cells showed a complex and ramified morphology, typical of more mature astrocytes (Fig. 3J).

We also immunolabeled for the cell proliferation marker Ki67 to estimate the fraction of proliferating Tomato+ astrocytes that may give rise to daughter cells through cell division events. This showed that Ki67+ proliferating astrocytes accounted for <10% of transplanted astrocytes at all time points examined (1, 3, 7, and 35–47 DPT; Fig. 3K). We also compared the number of Tomato+ astrocytes per section between brains collected at 7 DPT and 368+ DPT. Importantly, we found no significant difference in the density of transplanted cells/section between these two time points, indicating that there is no significant loss of transplanted astrocytes by 368 DPT (Fig. 3L).

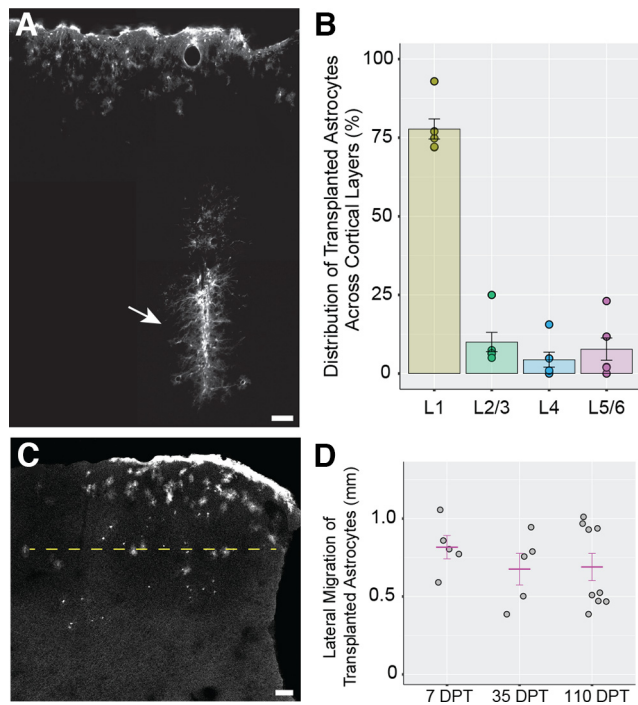


Figure 2. Distribution of transplanted Tomato+ astrocytes in cortex. **A**, Image montage representing the injection track (arrow) in a transplanted cortex at 35–47 DPT. **B**, Distribution of transplanted astrocytes across cortical layers at 35–47 DPT. Circles represent mean astrocyte number values per mouse for each layer region. L1 = layer 1, L2/3 = layers 2 and 3, L4 = layer 4, L5/6 = layers 5 and 6. **C**, The lateral migration distance (LMD; yellow dashed line) was defined as the maximum distance between transplanted astrocytes measured along the medio-lateral axis in sections without an injection track. In sections with injection track, the lateral migration distance was measured on the direction perpendicular to the injection track (data not shown). **D**, Lateral migration distance of transplanted astrocytes at different times post-transplantation. 35 DPT = 35–47 DPT, 110 DPT = 110–130 DPT. Gray circles represent mean LMD values per mouse. The mean LMD for each experimental group (magenta lines) are 0.816 ± 0.075 mm at 7 DPT, 0.676 ± 0.101 mm at 35–47 DPT, and 0.689 ± 0.087 mm at 110–130 DPT. No significant differences were detected between LMD values across post-transplantation times ($p = 0.562$, one-way ANOVA). Scale bar: 50 μ m (**A**) and 100 μ m (**C**). Data are mean \pm SEM.

Transplanted astrocytes develop unique morphologic territories and have normal levels of GFAP

Recent studies have shown that astrocytes can display scavenging activity toward damaged cells, opening the possibility that astrocytes phagocytize cellular material from adjacent astrocytes (Wakida et al., 2018). In light of these findings, it was important to determine whether some Tomato+ cells in recipient brains had acquired Tomato labeling by engulfing fragments of injected cells. At the same time, it was important to establish whether transplanted astrocytes could form mutually exclusive territories or “tile” the brain neuropil like astrocytes in normal brain (Ogata and Kosaka, 2002; Bushong et al., 2004). To answer these questions, we transplanted Tomato+ astrocytes into Aldh1l1-eGFP mice which express GFP specifically in astrocytes (Fig. 4A–C). To quantify the overlap between the territories of Tomato+ and GFP+ astrocytes, we acquired images containing both transplanted and nontransplanted astrocytes and calculated the degree of colocalization using Manders’ coefficients (M1 and M2). M1 and M2 represent the fraction of GFP signal colocalized with Tomato and the fraction of Tomato signal colocalized with GFP, respectively. The mean values of these coefficients across all mice (0.037 ± 0.009 for M1 and 0.065 ± 0.014 for M2) indicated that the overlap between transplanted and resident

astrocytes constituted $<10\%$ of the total area covered by Tomato+ and GFP+ astrocytes (Fig. 4D). This small amount of overlap is in line with that described for adjacent astrocytes in the brain of adult mice (Ogata and Kosaka, 2002). To further validate these results, we calculated the Manders’ coefficients values for astrocytic signals that are expected to display a high degree of overlap. For this, we chose Tomato and the astrocyte marker glutamine synthetase (GS), because both proteins are expressed in the astrocytic cytoplasm. In these measurements, M1 represents the fraction of GS signal colocalized with Tomato, while M2 represents the fraction of Tomato signal colocalized with GS. The mean values obtained for the two coefficients (0.316 ± 0.019 for M1 and 0.956 ± 0.013 for M2; Fig. 4E) were larger than those describing the overlap between Tomato+ transplanted and GFP+ nontransplanted astrocytes. A value lower than 1 for M1 is in line with the fact that in each field used for the coefficient calculation, only transplanted astrocytes expressed both Tomato and GS, and they occupied only a fraction (50% or less) of the field. The M2 value was very close to 1 indicating that Tomato and GS signals overlap almost completely in Tomato+ cells. These results showed that transplanted astrocytes acquired cortical space and formed complementary territories with GFP+ astrocytes. Furthermore, these data confirmed that Tomato+ cells were truly transplanted astrocytes uptake Tomato, which would complicate interpretation of the findings (Coyné et al., 2006).

To better understand whether transplanted astrocytes replace astrocytes from recipient mice or simply interlace among these cells, we compared the density of astrocytes for cortical regions which received astrocyte transplantation versus the contralateral cortex as a control. Interestingly, we found that astrocytic density was significantly higher in the transplanted cortex compared with the contralateral cortex (ratio of astrocyte density in transplanted/contralateral cortex = 1.66 ± 0.14 , $p = 0.021$, Wilcoxon rank-sum test; data not shown), indicating that astrocytes were more densely packed in the transplanted cortex. Thus, while transplanted astrocytes do establish cortical territories that “tile” with adjacent astrocytes (transplanted or nontransplanted), they do so by adding to the complement of astrocytes in the recipient cortex.

In response to challenges to the CNS, astrocytes undergo several morphologic, molecular, and functional changes and adopt a reactive phenotype (Escartin et al., 2021). One hallmark of astrocyte reactivity is the up-regulation of glial fibrillary acidic protein (GFAP). In normal conditions, this intermediate filament component is expressed sporadically in subsets of cortical astrocytes, including those located at the glial limitans in the outermost layer of the cortex, and those contacting brain vasculature at their endfeet (Lewis and Cowan, 1985; Kacem et al., 1998). In the presence of brain injury or disease, reactive astrocytes increase GFAP expression, particularly at the injury site or at the core of inflammation/cellular degeneration areas.

We were interested in determining whether transplanted astrocytes displayed aspects of a reactive phenotype. We found that transplanted astrocytes showed generally low levels of GFAP. To quantitatively assess this, we compared GFAP intensity between transplanted and nontransplanted astrocytes at 110–130 DPT. We identified regions of interest occupied by transplanted and nontransplanted astrocytes in confocal microscopy images (Fig. 4F) and calculated the transplanted/nontransplanted ratio for GFAP immunofluorescence. Since basal levels of GFAP in the cortex vary depending on the distance of astrocytes from the pia membrane (Fig. 4H), we selected a region of interest for a nontransplanted

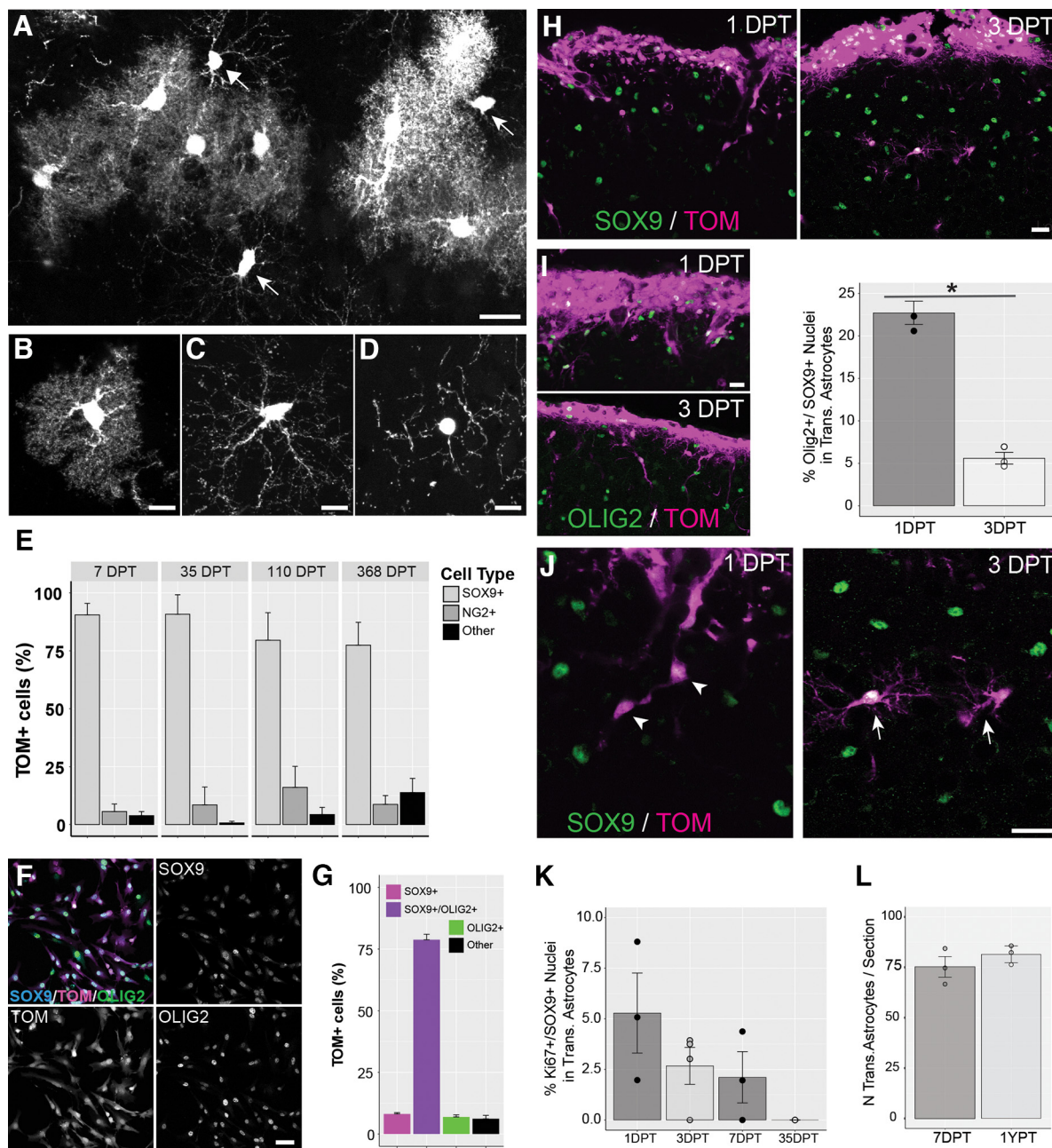


Figure 3. Characterization of transplanted cells. **A–D**, While most transplanted Tomato+ cells display a protoplasmic astrocytic morphology (**B**), some display less ramified, longer processes typical of oligodendrocyte precursor cells (**C**, OPCs; see also arrows in **A**) or immature oligodendrocytes (**D**). **E**, Cell-specific markers were used to identify the percentage of transplanted cells as Sox9+ astrocytes (**B**), NG2+ OPCs (**C**), or cells not expressing either Sox9 or NG2 referred to as “other” cells (**D**). **F**, Cultured cells expressing Sox9 and the glial precursor marker Olig2. Tom = Tomato. **G**, Percentage of TOM+ cultured cells positive for Sox9 only, Sox9 and Olig2, or Olig2 only. Cells not expressing either Sox9 or Olig2 were referred to as “other” cells. **H**, Sox9 expression in transplanted cells at 1 DPT and 3 DPT. **I**, Left panels, Olig2 expression in transplanted cells at 1 DPT and 3 DPT. Right panel, Percentage of Olig2+ cells among transplanted astrocytes at 1 DPT and 3 DPT. Circles and bars represent mean values per mouse and mean values per group, respectively. The percentage of Olig2+/Sox9+ cells among transplanted astrocytes was significantly lower at 3 DPT compared with 1 DPT (1 DPT, 22.73 ± 1.37 ; 3 DPT 5.6 ± 0.7 ; $*p = 0.0004$ Student’s *t* test). **J**, Most transplanted astrocytes have a simple, fusiform shape at 1 DPT (arrowhead), and take on a ramified stellate morphology at 3 DPT (arrow). **K**, Quantification of cell proliferation (Ki67+ nuclei) among transplanted astrocytes at different times after transplantation. Circles represent mean values per mouse. The mean values per experimental group (bars) are $7.21 \pm 2.38\%$ at 1 DPT, $2.67 \pm 0.91\%$ at 3 DPT, $2.11 \pm 1.26\%$ at 7 DPT and 0 at 35–47 DPT. Significant differences were not detected between the mean values per experimental group across times post-transplantation ($p = 0.09$, one-way ANOVA). **L**, Number of transplanted astrocytes per section at 7 DPT and 368–570 DPT (1 YPT). Circles and bars represent mean values per mouse and mean values per group, respectively. Scale bar: 20 μm (**A**, **H–J**), 10 μm (**B–D**), and 50 μm (**F**). Data are mean \pm SEM.

astrocyte that closely associated with that of the transplanted astrocyte. We also ensured that the two regions of interest were at a similar distance from the site where transplanted cells had been injected, as this region may be populated by clusters of reactive astrocytes displaying very high levels of GFAP (Fig. 4I). The mean transplanted/nontransplanted ratio for GFAP across all mice was not significantly different

from 1 (1.007 ± 0.018 ; Fig. 4G), indicating that transplanted astrocytes displayed similar levels of GFAP to nontransplanted astrocytes. This low level of GFAP expression in transplanted astrocytes, combined with their typical protoplasmic morphology and with absence of morphologic hypertrophy (Fig. 1G), suggested that transplanted astrocytes were not constitutively in a reactive state.

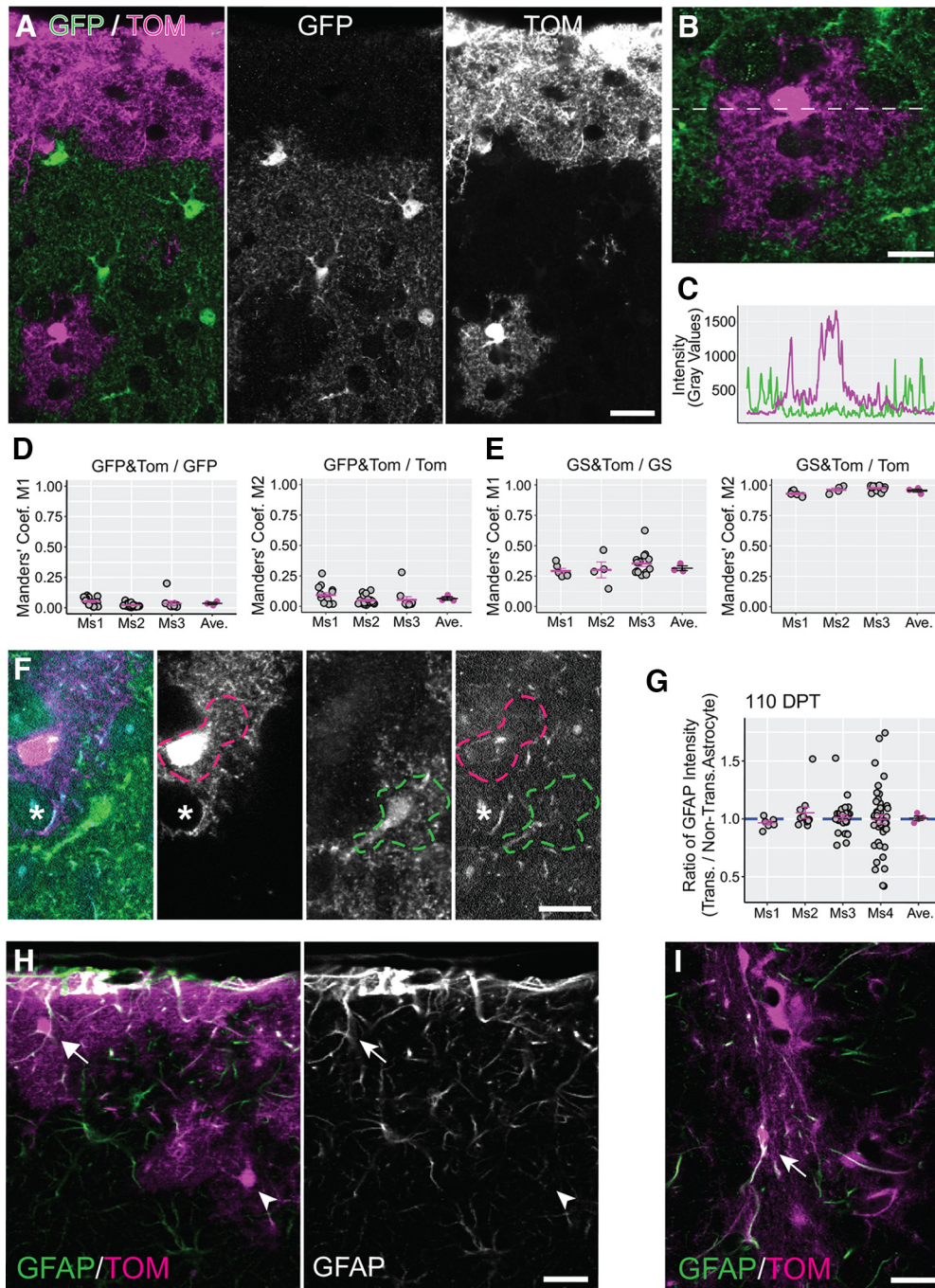


Figure 4. Transplanted astrocytes develop unique morphologic territories and have normal levels of GFAP. **A**, In the cortex of transplanted Aldh1L1-eGFP mice, the GFP+ and Tomato+ astrocytes show complementary organization. Tom = Tomato. **B**, **C**, Intensity values for GFP and Tomato signals were measured along a line drawn across adjacent transplanted and resident astrocytes. GFP and Tomato intensity profiles showed little overlap between the two signals (**C**). **D**, **E**, Manders' coefficients representing colocalization between GFP and Tomato (**D**) and colocalization between glutamine synthetase (GS) and Tomato (**E**) calculated for three mice (Ms1–Ms3) at 35–47 DPT. Gray circles are Manders' coefficient values calculated for single image fields, whereas lines represent mean coefficient values computed for each transplanted mouse (magenta) and across all mice in the same experimental group (black). In **D**, M1 and M2 represent the fraction of GFP signal colocalized with Tomato (GFP&TOM/GFP) and the fraction of Tomato signal colocalized with GFP (GFP&TOM/TOM), respectively. In **E**, M1 and M2 represent the fraction of glutamine synthetase (GS) signal colocalized with Tomato (GS&TOM/GS) and the fraction of Tomato signal colocalized with GS (GS&TOM/TOM), respectively. **F**, GFAP expression levels were compared between transplanted (magenta dashed line) and nontransplanted astrocytes (green dashed line) by measuring GFAP intensity in territories occupied by the two kinds of astrocytes. Astrocytic processes that were potentially identified as endfeet (asterisk) were excluded from the quantification. **G**, Transplanted/nontransplanted ratio values for GFAP expression calculated for single image fields (gray circles) in four mice (Ms1–Ms4) at 110–130 DPT. Magenta lines/circles represent mean values per mouse. The mean value across all mice (black line) was not significantly different from 1 (1.007 ± 0.018 ; $p = 1$, Wilcoxon rank-sum test). **H**, GFAP immunolabeling at 35–47 DPT in the superficial layer of the cortex (mouse transplanted at P3–P7). Similar to nontransplanted astrocytes, transplanted astrocytes displayed high GFAP levels close to the pial membrane (arrow) and lower GFAP levels deeper in cortex (arrowhead). **I**, GFAP immunolabeling at 35–47 DPT at the injection site (mouse transplanted at P3–P7). Transplanted astrocytes express high levels of GFAP at the injection site (arrow). Scale bar: 20 μm (**A**, **H**, **I**) and 10 μm (**B**, **F**). Data are mean \pm SEM.

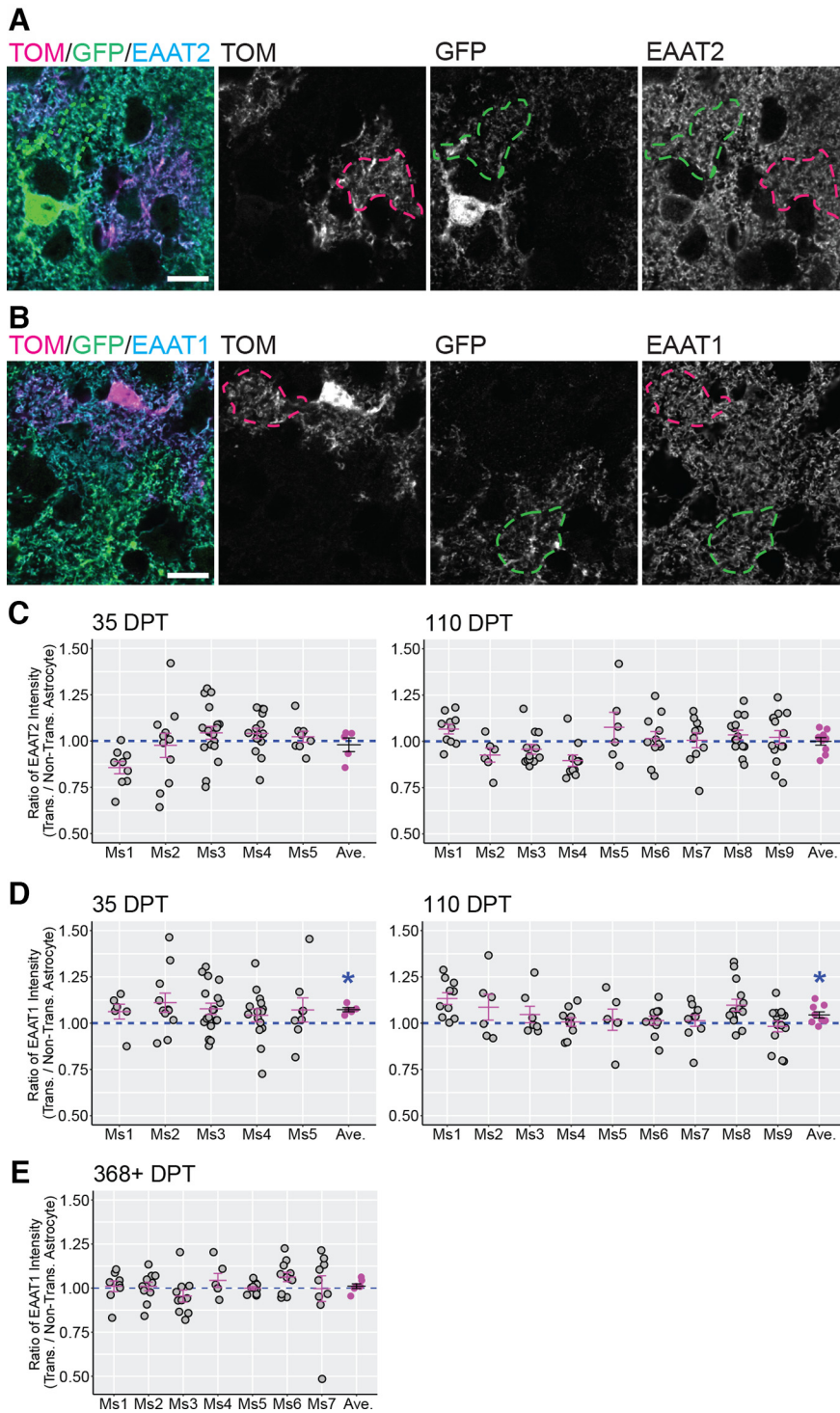


Figure 5. Expression of glutamate transporters EAAT2/GLT1 and EAAT1/GLAST in transplanted and nontransplanted astrocytes. **A, B**, Representative ROIs used to measure EAAT2/GLT1 (**A**) and EAAT1/GLAST (**B**) intensity in territories occupied by transplanted (magenta dashed line) and nontransplanted (green dashed line) astrocytes. Tom = Tomato. **C–E**, Transplanted/nontransplanted ratio values for GLT1 and GLAST at different times after transplantation. Ratio values for both glutamate transporters were calculated at 35–47 DPT and at 110–130 DPT (**C, D**), and an additional time point for GLAST was added at 368–570 (368+) DPT (**E**). Gray circles and magenta lines/circles represent ratio values per image field, and mean ratio values per mouse (Ms), respectively. The mean ratio values for each experimental group (black lines) are 0.979 ± 0.037 for GLT1 at 35–47 DPT ($p = 0.656$, Wilcoxon rank-sum test), 1 ± 0.020 for GLT1 at 110–130 DPT ($p = 0.22$, Wilcoxon rank-sum test), 1.073 ± 0.011 for GLAST at 35–47 DPT ($*p = 0.007$, Wilcoxon rank-sum test), 1.044 ± 0.017 for GLAST at 110–130 DPT ($*p = 0.003$, Wilcoxon rank-sum test), and 1.011 ± 0.013 for GLAST at 368–570 DPT ($p = 0.68$, Wilcoxon rank-sum test). Scale bar: $10 \mu\text{m}$ (**A, B**). Data are mean \pm SEM.

Transplanted astrocytes express similar levels of glutamate transporter EAAT2/GLT1 but show elevated levels of EAAT1/GLAST that resolve after one year *in vivo*

Having observed that transplanted astrocytes develop morphologic properties that match nontransplanted astrocytes in the cortex of recipient mice, we next investigated the molecular features of transplanted astrocytes. Glutamate transporters, also named excitatory amino acid transporters (EAATs), are expressed by astrocytes and neurons in the brain. EAAT2/GLT1 and EAAT1/GLAST are abundant transporters observed in astrocytes and play an important role in removing extracellular glutamate (Sattler and Rothstein, 2006; Rose et al., 2018). To determine whether transplanted astrocytes expressed levels of EAAT2/GLT1 and EAAT1/GLAST similar to nontransplanted astrocytes, we immunolabeled for each glutamate transporter and acquired images containing both Tomato+ transplanted astrocytes and neighboring nontransplanted astrocytes (Fig. 5A,B). For each image field we calculated the ratio between the EAAT2/GLT1 or EAAT1/GLAST intensity measured in the transplanted versus adjacent nontransplanted astrocyte (Fig. 5C–E). For EAAT2/GLT1, the mean transplanted/nontransplanted ratio was not significantly different from 1 at either 35–47 DPT (0.979 ± 0.037 ; Fig. 5C) or 110–130 DPT (1 ± 0.020 ; Fig. 5C), indicating that this glutamate transporter was expressed in comparable amounts by transplanted and nontransplanted astrocytes as early as 35–47 DPT. For EAAT1/GLAST, the mean transplanted/nontransplanted ratio across all mice in the same experimental group was significantly higher than 1 at 35–47 DPT (1.073 ± 0.011 ; Fig. 5D) and at 110–130 DPT (1.044 ± 0.017 ; Fig. 5D). To understand whether the increase was sustained long-term, we analyzed the transplanted/nontransplanted ratio for EAAT1/GLAST at 368–570 DPT. However, by this time, the transplanted/nontransplanted ratio normalized and was not different from 1 (1.011 ± 0.013 ; Fig. 5E). This indicated that transplanted astrocytes expressed higher levels of EAAT1/GLAST compared with nontransplanted astrocytes during the few months following transplantation. However, this upregulation resolved at later time points. EAAT2/GLT1 expression levels, in contrast, remained similar between transplanted and nontransplanted astrocytes at all time points analyzed. Overall, these

results showed that transplanted astrocytes acquired and retained levels of EAAT expression similar to nontransplanted astrocytes.

Transplanted astrocytes acquire layer-specific expression of GFAP and Kir4.1

Cortical astrocytes display heterogeneous gene expression patterns associated with cortical layering (Lanjakornsiripan et al., 2018; Batiuk et al., 2020; Bayraktar et al., 2020). We were interested to know whether astrocytes acquire layer-specific molecular features following their transplantation. We first assessed astrocyte heterogeneity in our cultures, by immunolabeling them for GFAP and for the potassium channel Kir4.1 (Fig. 6A), an astrocytic marker that displays complementary expression pattern to GFAP *in vivo* in mouse cortex. In the mouse cortex, GFAP is predominantly expressed in layer 1, whereas Kir4.1 is more abundantly expressed in lower layers. We found that GFAP and Kir4.1 signal intensity for Tomato⁺ cells in our cultures showed some variable expression across culture batches (Fig. 6B,C), but did not show inversely correlated expression patterns (Fig. 6D). We then quantified GFAP and Kir4.1 expression levels in transplanted and nontransplanted astrocytes at 35–47 DPT (Fig. 6E–H) and observed that transplanted astrocytes, like nontransplanted astrocytes, express higher levels of GFAP in layer 1 of cortex compared with astrocytes positioned in layers 2–3 (Fig. 6E,F). Transplanted astrocytes also displayed expression of Kir4.1 similar to nontransplanted astrocytes, with higher expression in layers 2–3 versus layer 1 (Fig. 6G,H). Thus, despite the lack of inverse expression of GFAP and Kir4.1 in culture, transplanted astrocytes acquire differential expression of GFAP and Kir4.1 *in vivo*.

Transplanted and nontransplanted astrocytes associate with similar numbers of excitatory and inhibitory presynaptic terminals

In the first three postnatal weeks, astrocytes in the mouse cortex undergo extensive growth and maturation. During this time, they actively participate in the formation, maturation, and maintenance of synapses by signaling to neurons through the release of diffusible factors (Allen and Eroglu, 2017; Tan et al., 2021) and creating tight contacts with presynaptic and postsynaptic sites. Thus, we were interested in determining whether transplanted astrocytes were associated with the same number of cortical synapses as nontransplanted astrocytes. To study this, we visualized presynaptic terminals by immunolabeling for the vesicular glutamate transporters 1 and 2 (vGLUT1 and vGLUT2) to label glutamatergic terminals, and vesicular GABA transporter (vGAT) to label GABAergic terminals. We next selected regions of interest on transplanted or nontransplanted astrocytes (Fig. 7A,B) and calculated the coverage by the synaptic labels (Fig. 7A–C). We then computed the transplanted/nontransplanted particle coverage ratio for each image field. Ratio values lower than one indicated lower density of presynaptic terminals in transplanted astrocytes compared with nontransplanted astrocytes, whereas values higher than one indicate higher presynaptic terminal density in transplanted astrocytes. At 110–130 DPT, the mean transplanted/nontransplanted presynaptic terminal particle ratio was not significantly different from 1 for either vGlut1/2 (1.117 ± 0.111 ; Fig. 7D) or vGAT particles (1.174 ± 0.09 ; Fig. 7E), indicating that transplanted and nontransplanted astrocytes were associated with similar numbers of excitatory and inhibitory presynaptic terminals. These results suggested that

astrocytic transplantation does not impair the ability of astrocytes to support synapse formation and maintenance.

Transplanted astrocytes express aquaporin 4 and gap junctional markers at endfeet, and display similar Ca²⁺ transients

Astrocytic endfeet are highly specialized perivascular structural compartments created by astrocytes that closely associate with the basement membrane, pericytes, vascular smooth muscle cells, and endothelial cells. Being located at the interface between the brain parenchyma and vasculature, endfeet mediate communication between these compartments, and play a fundamental role in neurovascular coupling and maintenance of the blood brain barrier (Cohen-Salmon et al., 2021; Stackhouse and Mishra, 2021). A typical feature of astrocytic endfeet is the high concentration of aquaporin 4 (AQP4), a water channel that mediates water exchange and clearance of brain interstitial fluid (Papadopoulos and Verkman, 2013; Mestre et al., 2020). To understand whether transplanted astrocytes concentrate AQP4 at endfeet near vasculature, we compared endfoot expression levels of AQP4 between transplanted and nontransplanted astrocytes within the same image field (Fig. 8A,B, magenta and green dashed lines) and calculated a ratio between these intensity values (transplanted/nontransplanted AQP4 ratio; Fig. 8C). Interestingly, this ratio was significantly lower than 1 at 35–47 DPT (0.812 ± 0.057), indicating a lower level of expression of AQP4 in transplanted astrocytes. However, this lower AQP4 expression normalized by 110–130 DPT (1.006 ± 0.045 ; Fig. 8C). We also assessed the presence of gap junctional subunits [Connexin 30 (CX30) and 43 (CX43)] that are known to be enriched at endfeet (Rash et al., 2001) and arranged in large puncta (Ezan et al., 2012). Co-immunolabeling for CX30 and CX43 at 35–47 DPT showed large CX30⁺ and CX43⁺ puncta at the endfeet of transplanted astrocytes, with the two gap junctional subunits frequently co-localized in these puncta (Fig. 8D). Thus, transplanted astrocytes concentrate AQP4 and gap junctional subunits at their endfeet.

To determine whether transplanted astrocytes show Ca²⁺ activity similar to nontransplanted astrocytes, we prepared acute cortical slices and monitored Ca²⁺ activity following bulk loading of the Ca²⁺ indicator Fluo-4AM. We analyzed the properties of spontaneous Ca²⁺ events in transplanted and nontransplanted astrocytes and found similar properties with respect to event area, $\Delta F/F$, duration, and decay (Fig. 8E,F). Overall, these results along with those from the endfoot analysis suggest that transplanted astrocytes display molecular and functional properties similar to those of nontransplanted astrocytes.

Cortical astrocytes transplanted to more mature brain survive but are largely retained at the transplantation site

Having found that cortical astrocytes integrate and survive following their transplantation to the immature brain, we next determined whether astrocytes display similar properties when transferred to the more mature brain. To address this, we injected astrocytes into the cortex of young adult mice (P34–P43; Fig. 9A) and tracked astrocyte integration at 35–47 DPT. We found that transplanted astrocytes survived in large numbers and maintained their astrocyte identity as confirmed by immunolabeling for Sox9 (Fig. 9B). However, transplanted astrocytes were largely confined to the transplantation site or at superficial layers of the cortex (Fig. 9B) and in some cases at a small distance from the injection site (Fig. 9B,F). We measured the ability of transplanted astrocytes to migrate away from the injection site and found that

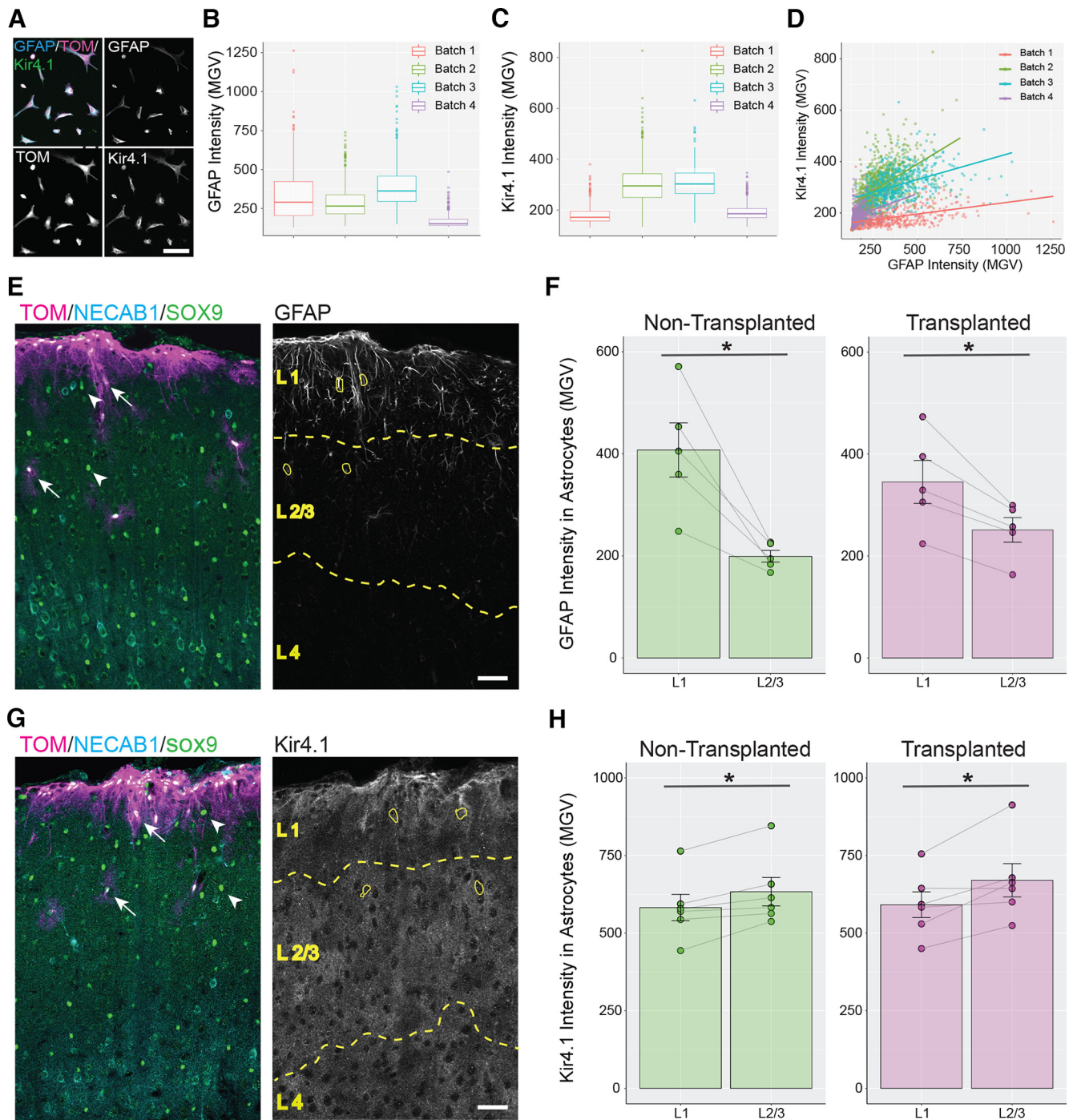


Figure 6. Transplanted astrocytes acquire layer-specific expression of GFAP and Kir4.1. **A**, Immunolabeling for GFAP and Kir4.1 in cultured astrocytes. Tom = Tomato. **B**, **C**, Distribution of GFAP (**B**) and Kir4.1 (**C**) intensity levels in four batches of cultured astrocytes. **D**, Plot of Kir4.1 intensity versus GFAP intensity for cultured astrocytes collected from four different batches. Colored lines represent the best-fit lines for each cell batch. **E–H**, Analysis of the distribution of GFAP and Kir4.1 *in vivo*. **E**, **G**, Necab1 and Sox9 immunolabeling were used to identify cortical layers (dashed yellow lines and captions; see Materials and Methods). L1 = layer 1, L2/3 = layers 2 and 3, L4 = layer 4. ROIs were created (yellow line) for transplanted (arrow) and nontransplanted (arrowhead) astrocytes, and for each ROI mean intensity values of GFAP (**E**) or Kir4.1 (**G**) were measured. **F**, **H**, For each mouse, the mean GFAP (**F**) or Kir4.1 (**H**) intensity values per mouse (circles) measured in L1 were compared with those measured in L2/3 (gray lines). **F**, The mean intensity value for GFAP was significantly higher in L1 compared with L2/3 for both nontransplanted (green, 407.47 ± 53.13 in L1, 199.28 ± 11.5 in L2; $p = 0.01$, paired Student's *t* test) and transplanted astrocytes (magenta, 345.35 ± 42.03 in L1, 251.31 ± 24.09 in L2; $p = 0.012$, paired Student's *t* test). **H**, The mean intensity value for Kir4.1 was significantly lower in L1 compared with L2/3 for both nontransplanted (green, 582.33 ± 42.48 in L1, 633.49 ± 45.76 in L2; $p = 0.013$, paired Student's *t* test) and transplanted astrocytes (magenta, 592.52 ± 42.23 in L1, 670.18 ± 53.51 in L2; $p = 0.028$, paired Student's *t* test). Scale bar: 100 μm (**A**) and 50 μm (**E**, **G**). Data are mean \pm SEM.

the lateral migration of transplanted astrocytes was significantly lower in mice transplanted at P34–P43 (adult transplantation) compared with mice transplanted at P3–P7 (developmental transplantation; Fig. 9G). Astrocytes transplanted at P34–P43

that remained at the injection site commonly displayed elongated shapes and thick processes containing high expression of GFAP consistent with a reactive phenotype (Fig. 9C,F). In some instances, transplanted astrocytes escaped the transplantation site

and were found to acquire a protoplasmic morphology (Fig. 9E,F). These cells also showed lower levels of GFAP expression (Fig. 9F). We also analyzed the expression of glutamate transporters EAAT2/GLT1 and EAAT1/GLAST in astrocytes transplanted at P34–P43. We found that transplanted and nontransplanted protoplasmic astrocytes express similar levels of these transporters at 110–130 DPT (transplanted/nontransplanted ratios: 0.937 ± 0.039 for EAAT2/GLT1, $p = 0.282$, Wilcoxon rank-sum test; 1.117 ± 0.111 for EAAT1/GLAST, $p = 0.282$, Wilcoxon rank-sum test). Interestingly, we did not detect significant differences in the expression of cleaved caspase 3 (an indicator of apoptotic cell death) between the adult and developmental transplantation groups, suggesting the absence of increased cell death following transplantation to more mature mice (Fig. 9H). Thus, transplantation of cortical astrocytes into more mature cortex results in heterogeneous astrocytic phenotypes with reactive astrocytes and protoplasmic astrocytes found near and distal to the transplantation site, respectively.

Transplanted cortical astrocytes integrate into the developing cerebellar cortex but retain cortical-like astrocytic features

Having shown that cortical astrocytes transplanted into developing cortex establish structural and molecular features similar to nontransplanted cortical astrocytes, we next asked whether cortical astrocytes can acquire the characteristics of nearby nontransplanted astrocytes if transplanted to a mismatched brain region. To answer this question, we transplanted cortical astrocytes into the cerebellum of P5–P8 mice (Fig. 10A) and tracked their development in the molecular layer (ML) of the cerebellar cortex where Bergmann glia (BG) extend highly polarized processes from the Purkinje cell (PC) layer to the pial surface (Yamada and Watanabe, 2002; Kita et al., 2013). In addition to these specific structural features, BG express high levels of the glutamate transporter EAAT1/GLAST (Farmer et al., 2016) and uniquely express the AMPA receptor subunit GluA1 (Saab et al., 2012).

At 21 DPT, we found many Tomato+/Sox9+ astrocytes in the cerebellar cortex (Fig. 10B). The cell bodies of these astrocytes were often found positioned superficially in the ML. Despite this abnormal cell body positioning, astrocytes elongated processes deeper within the ML (Fig. 10B). In areas where the density of transplanted astrocytes was lower, we observed that they displayed a less-polarized, stellate shape reminiscent of cortical astroglia (compare Fig. 10B, arrow, with 1G). Interestingly, transplanted astrocytes showed low to undetectable levels of GluA1 and lower levels of EAAT1/GLAST compared with nearby BG cells (Fig. 10C,E). Measuring the signal intensity

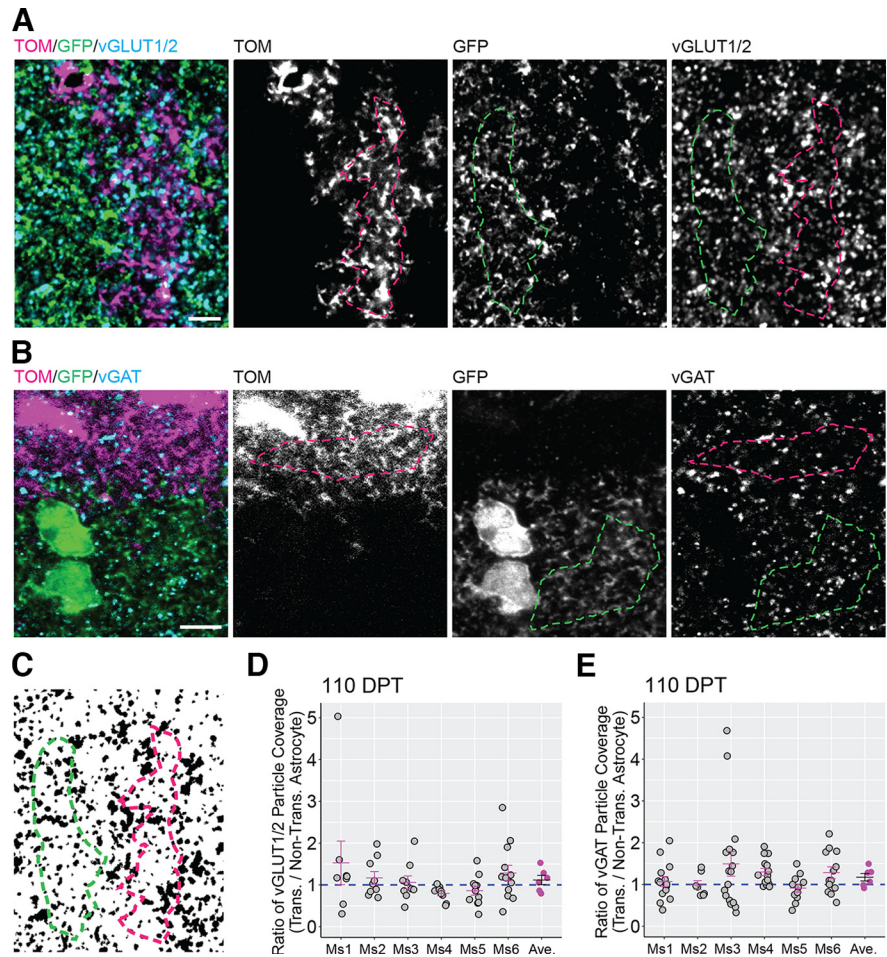


Figure 7. Transplanted and nontransplanted astrocytes are associated with similar numbers of excitatory and inhibitory presynaptic terminals. **A, B**, To assess presynaptic particle coverage in transplanted (magenta dashed line) and nontransplanted astrocytes (green dashed line), territories occupied by either kind of astrocytes were identified in sections labeled for vGLUT1/2 (excitatory presynaptic terminals) or vGAT (inhibitory presynaptic terminals). Tom = Tomato. **C–E**, In binary images derived from vGLUT1/2 and vGAT image channels (**C**), the ratio values between the particle coverage of transplanted and nontransplanted astrocytes (transplanted/nontransplanted particle coverage ratio) were calculated per image fields (gray circles) and per mouse (Ms, magenta lines/circles). The mean transplanted/nontransplanted particle coverage ratio across all mice (black line) was not significantly different from 1 for either vGLUT1/2 (1.117 ± 0.111 ; $p = 0.347$, Wilcoxon rank-sum test) or vGAT (1.174 ± 0.09 ; $p = 0.347$, Wilcoxon rank-sum test). Scale bar: $5 \mu\text{m}$ (**A, B**). Data are mean \pm SEM.

profiles across the ML revealed a steep increase of GluA1 and EAAT1/GLAST levels at the interface between transplanted cells and nontransplanted BGs (Fig. 10D,F). Transplanted astrocytes also retained higher levels of EAAT2/GLT1 (Fig. 10E). These results suggested that transplanted cortical astrocytes integrate and develop in the cerebellar cortex, but retain structural and molecular features of cortical astrocytes.

BG develop in close association with PCs, and BG processes have been proposed to function as scaffold for the elongation of PC dendrites in the first postnatal weeks (Lordkipanidze and Dunaevsky, 2005). Given that transplanted cortical astrocytes lacked the specialized morphology and molecular phenotype of BG, we wondered whether they could provide a favourable environment for the growth and maintenance of PC dendritic arbors. We visualized PC dendrites through Calbindin immunolabeling, and observed that PC dendrites elongated normally on territories occupied by cortical astrocytes (Fig. 10G). This suggested that astrocytes derived from cortex can replace BG arbors without noticeable effects on Purkinje cell dendritic branching.

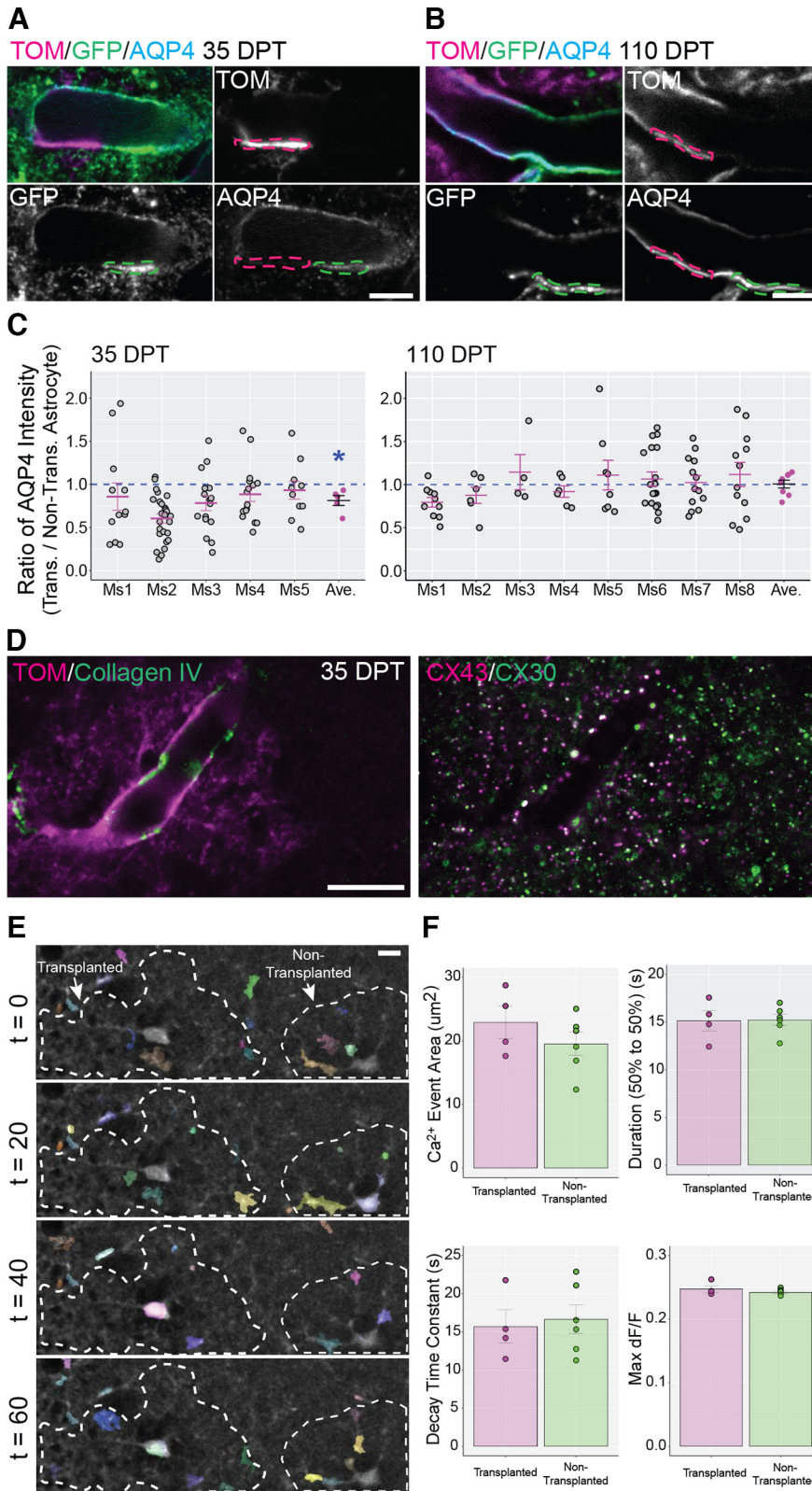


Figure 8. Transplanted and nontransplanted astrocytes express aquaporin 4 and gap junction proteins at endfeet and display similar properties of Ca^{2+} events. **A–C**, The expression level of the water channel aquaporin 4 (AQP4) was compared between transplanted and nontransplanted astrocytes at 35–47 DPT and 110–130 DPT. Tom = Tomato. **A, B**, AQP4 intensity was measured in endfeet from transplanted astrocytes (magenta dashed line) and adjacent endfeet from nontransplanted astrocytes (green dashed line). **C**, The ratio for AQP4 intensity at endfeet (transplanted/nontransplanted AQP4 ratio) was calculated for single image fields (gray circles), for each transplanted mouse (Ms, magenta lines/circles), and across all mice in the same experimental group (black lines). The mean value of this ratio was significantly lower than 1 at 35–47 DPT (0.812 ± 0.057 ; $*p = 0.007$, Wilcoxon rank-sum test) but was not significantly different from 1 at 110–130 DPT

Transplanted cerebellar astrocytes develop both Bergmann glia and velate-like astrocytic properties in the cerebellum

Finally, we investigated whether transplanting cerebellar astrocytes into cerebellum can generate appropriate cerebellar astrocytic phenotypes. Astrocyte maturation in the cerebellar cortex is a highly regulated and timed process that gives rise to two main regionally specialized astrocyte types, namely, BG in the ML and velate astrocytes in the granule cell layer (GCL; Farmer et al., 2016). In contrast to BGs, velate astrocytes have more stellate morphology and form sheath-like processes around granule cells. Velate astrocytes, unlike BGs, also have low levels of GluA1 but have high levels of AQP4 (Yamada and Watanabe, 2002; Kita et al., 2013). We transplanted cerebellar astrocytes into the cerebellum of P5–P8 mice (Fig. 11A). Interestingly, at 21 DPT, astrocytes transplanted in the ML showed distinct morphologies with thick radial shafts extending from the cell body toward the pial surface (Fig. 11B,C), mimicking a major structural property of BGs. Cerebellar astrocytes transplanted in the ML also expressed GluA1 and displayed low levels of AQP4 (Fig. 11D,E). Conversely, cerebellar astrocytes transplanted deeper into the GCL showed morphologies similar to velate astrocytes, and did not express noticeable levels of GluA1 (Fig. 11F). However, these cells showed high levels of AQP4 (Fig. 11G). These findings showed that cerebellar astrocytes behave differently than cortical astrocytes when transplanted into the developing

(1.006 ± 0.045 ; $p = 0.4$, Wilcoxon rank-sum test). **D**, The endfoot of a transplanted astrocyte (Tom, left panel) in contact with a blood vessel labeled for Collagen IV (left panel) enriched with large aggregates of Connexin 43 (CX43) and Connexin 30 (CX30; right panel). **E**, Ca^{2+} events were recorded in cortical slices prepared from transplanted mice in a field containing a transplanted and nontransplanted astrocyte (dashed lines). Ca^{2+} event recordings were processed for noise reduction and analyzed using AQuA. Ca^{2+} events were detected (colored regions) in the soma and processes of both transplanted and nontransplanted astrocytes. **F**, Ca^{2+} event area, duration, decay time, and maximum deltaF/F were calculated. No significant differences were detected between transplanted and nontransplanted astrocytes (Ca^{2+} event area: 19.53 ± 1.83 for nontransplanted cells, 22.93 ± 2.55 for transplanted cells, $p = 0.296$, Student's t test; Duration: 15.22 ± 0.59 for nontransplanted cells, 15.15 ± 1.07 for transplanted cells, $p = 0.949$ Student's t test; Decay time constant: 16.65 ± 1.88 for nontransplanted cells, 15.76 ± 2.18 for transplanted cells, $p = 0.767$ Student's t test; Max dF/F: 0.242 ± 0.002 for nontransplanted cells, 0.247 ± 0.005 for transplanted cells, $p = 0.286$, Student's t test). Scale bar: 5 μ m (**A, B**) and 10 μ m (**D, E**). Data are mean \pm SEM.

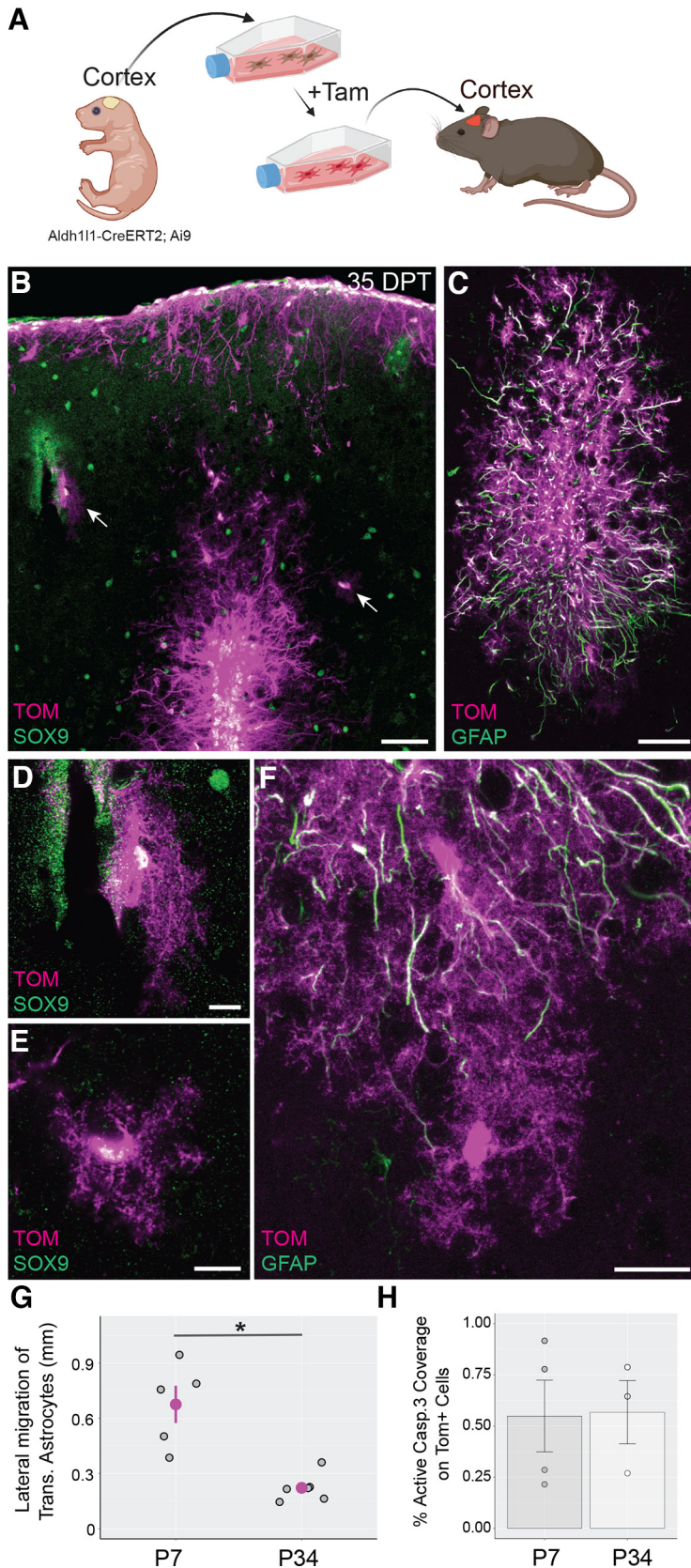


Figure 9. Cortical astrocytes transplanted to the more mature mouse brain survive but generally fail to escape the injection site. **A**, Overview of the experimental design for transplantation of cortical astrocytes into the cerebral cortex of young adult mice (P34–P43). Tam = 4-hydroxytamoxifen. Figure created with BioRender. **B–E**, At 35–47 d post-transplantation (DPT), most transplanted astrocytes were accumulated around the injection site, had elongated morphologies typical of reactive astrocytes, and displayed high expression of GFAP (**C**). Some of these cells displayed

cerebellum, acquiring the unique properties of cerebellar astrocytes.

Discussion

In this study, we investigated how transplanted cortical astrocytes integrate, mature, and survive in the brain. We found that cortical astrocytes transplanted into the developing cortex of mice acquired structural, molecular, and functional features similar to nontransplanted astrocytes in the recipient cortex. The properties of transplanted cortical astrocytes closely resembled nontransplanted astrocytes of recipient mice including their ability to form complex architectures, form mutually exclusive territories, develop endfeet on vasculature, and support synapse formation/maintenance. Importantly, astrocytes maintained these properties beyond one year *in vivo*. In contrast, immature cortical astrocytes transplanted into more mature cortex (postnatal days 34–43) elaborated their morphology, but had limited capacity to disperse beyond the transplantation site into the recipient cortex and, in many instances, had structural and molecular properties of reactive astrocytes. Interestingly, immature cortical astrocytes retained their cortical astrocyte-like features even when nurtured in the developing cerebellar cortex, indicating strong intrinsic mechanisms driving their structural maturation and gene expression.

Accumulating evidence suggests that astrocytes are molecularly, structurally, and functionally heterogeneous, with properties that vary depending on developmental origin, cell positioning, and sensitivity to environmental cues (Ben Haim and Rowitch, 2017; Farmer and Murai, 2017). Single-cell RNA-seq and transcriptomic mapping have revealed significant molecular heterogeneity of astrocytes in the rodent cortex (Batiuk et al., 2020; Bayraktar et al., 2020). Interestingly, studies have shown that transcription factor patterning is important for specifying astrocytic populations in the mouse spinal cord by embryonic day (E)18.5 (Hochstim et al., 2008) and in cortex by postnatal day 4 (P4;

protoplasmic astrocytic morphology (**B**, arrows; **D**, **E**) and displayed low levels of GFAP (**F**). Tom = Tomato. **G**, Lateral migration of transplanted astrocytes in mice transplanted at P3–P7 (P7) and analyzed at 35–47 DPT, and mice transplanted at P34–P43 (P34) and analyzed at 35–47 DPT. Gray circles represent mean lateral migration distance (LMD) values per mouse. The mean LMD value for the P7 group was significantly lower than that for the P34 group (magenta circles, P7, 0.676 ± 0.101 mm; P34, 0.222 ± 0.031 mm; $*p = 0.009$, Student's *t* test). **H**, Expression of activated caspase 3 by transplanted astrocytes in mice transplanted at P3–P7 (P7) and analyzed at 1 DPT and mice transplanted at P34–43 (P34) and analyzed at 1 DPT. Circles and bars represent mean values of active caspase 3 coverage per mouse and per experimental group, respectively. No significant differences were detected between P7 and P34 (P7, $0.55 \pm 0.17\%$; P34, $0.57 \pm 0.15\%$; $p = 0.942$, Student's *t* test). Scale bar: 50 μ m (**B**, **C**), 10 μ m (**D**, **E**), and 20 μ m (**F**). Data are mean \pm SEM.

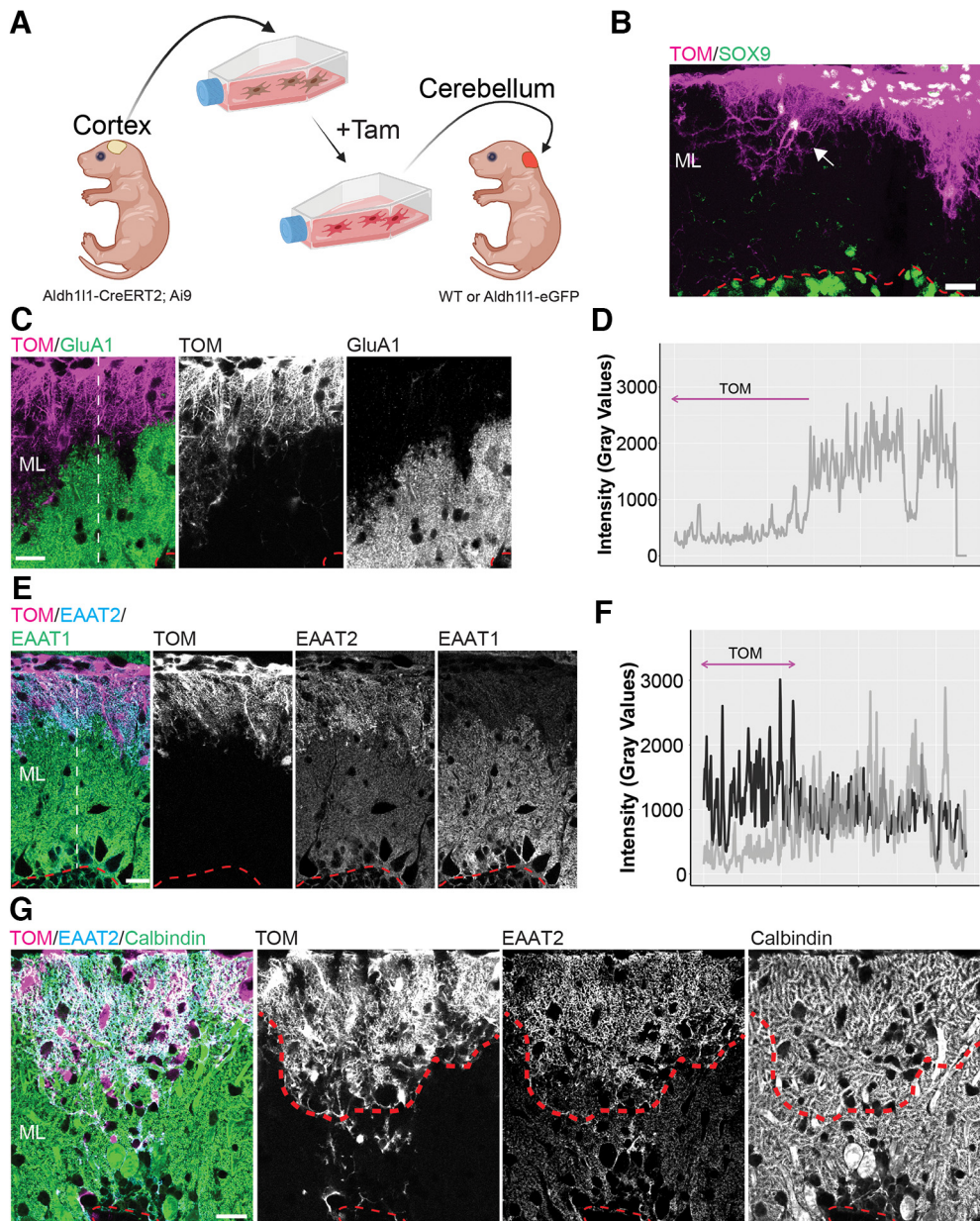


Figure 10. Transplanted cortical astrocytes integrate into the cerebellar cortex but retain structural and molecular features of cortical astrocytes. **A**, Overview of the experimental design for transplantation of cortical astrocytes into the cerebellum of mouse pups. *Tam* = 4-hydroxytamoxifen. Figure created with BioRender. **B**, Most astrocytes transplanted in the molecular layer (ML) remained confined in the subpial region of the cerebellar cortex and extended process deeper into the ML. Some transplanted astrocytes showed a stellate shape similar to cortical protoplasmic astrocytes (arrow). **C–F**, Transplanted cortical astrocytes expressed lower amounts of the AMPA-type glutamate receptor subunit GluA1 and glutamate transporter EAAT1/GLAST compared with nearby Bergmann glia but maintained high levels of EAAT2/GLT-1. Radial lines were drawn in the ML across transplanted astrocytes and adjacent BG cells (white dashed lines, **C**, **E**) to identify sites of intensity profile measurements for GluA1 (**D**), EAAT1 (**F**, gray), and EAAT2 (**F**, black). The region occupied by transplanted astrocytes (magenta line **D**, **F**, black) was associated with low levels of GluA1 and EAAT1 and high levels of EAAT2, whereas the region occupied by BG displayed complementary intensity profiles for the three markers. **G**, The presence of cortical astrocytes in the ML did not interfere with the growth or maintenance of Purkinje cell (PC) dendrites. The direction of PC dendrites did not change at the interface between transplanted cortical astrocytes and BG cells (thick red dashed line). Tom = Tomato. **B**, **C**, **E**, **G**, A thin red dashed line indicates the border between the ML and the PC layer. Scale bar: 50 μ m (**B**) and 20 μ m (**C**, **E**, **G**).

Tsai et al., 2012). At the same time, other studies have shown that local, non-cell-autonomous factors further diversify astrocytes to appropriately configure them for local brain microenvironments (Farmer et al., 2016). Our experiments show that specific features of cortical astrocytes are already in place during the first postnatal week. Moreover, these features are highly resilient, serving to maintain cortical astrocyte-like properties even when astrocytes are subjected to brain extraction, *in vitro* growth conditions, and transplantation to a foreign brain region such as the cerebellar cortex. What imparts this resiliency of cortical astrocytes? Studies have

shown that cortical astrocytes exhibit distinctive epigenetic signatures (Welle et al., 2021) and are enriched in particular histone variants and chromatin modifiers which may promote and repress transcription (Bargaje et al., 2012; Rege et al., 2015). The continued expression of these histone and chromatin modifiers may maintain cortical astrocytic specification state even under significant environmental challenges. This resembles results from cell transplantation experiments performed in the embryonic ferret brain showing that intrinsic determinants strongly restrict the fate of neuronal precursors (Frantz and McConnell, 1996). Further research will be required to pinpoint the developmental

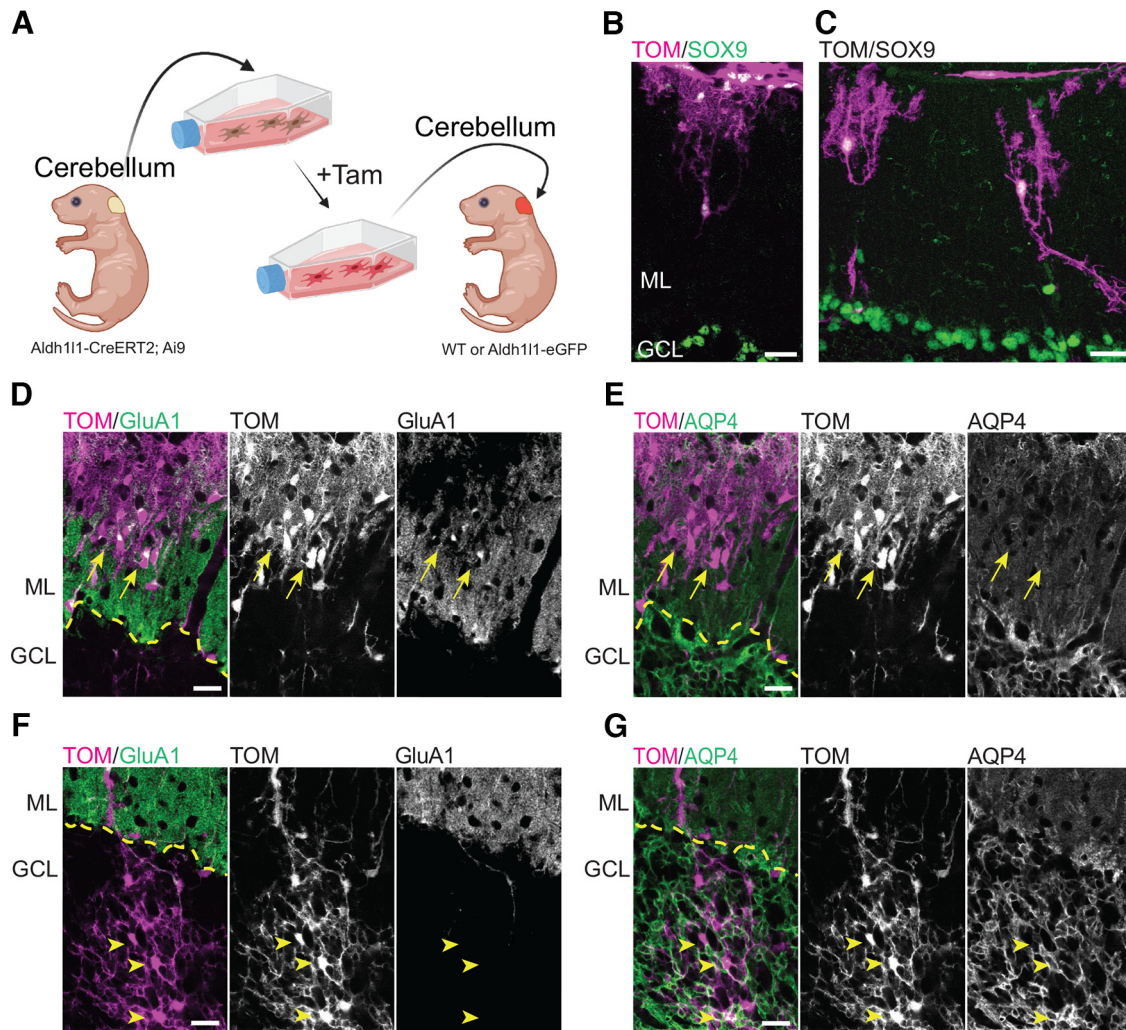


Figure 11. Cerebellar astrocytes develop into Bergmann glia-like and velate-like astrocytes when transplanted into the cerebellum. **A**, Overview of the experimental design for transplantation of cerebellar astrocytes into the cerebellum of mouse pups. *Tam* = 4-hydroxytamoxifen. Figure created with BioRender. **B–G**, Cerebellar astrocytes transplanted in the cerebellar cortex acquired region-specific structural and molecular features. **B**, **C**, Transplanted cerebellar astrocytes located in the ML display BG-like morphologies. **D**, **E**, Astrocytes transplanted in the ML (arrows) express GluA1 and low levels of AQP4, like BG cells. **F**, **G**, Astrocytes transplanted in the granule cell layer (GCL; arrowheads) display a velate-like astrocytic morphology and, like velate astrocytes, are negative for GluA1 and express high levels of AQP4. Tom = Tomato. Scale bar: 20 μ m (**B–G**). Dashed yellow line marks the interface between ML and GCL.

stage when cortical astrocytes establish specific signatures and whether reprogramming methods before transplantation can modify these signatures and ultimately the fate of transplanted cells.

Our results show a small mismatch in some molecular properties of transplanted and nontransplanted astrocytes. We found that EAAT1/GLAST expression was higher in transplanted astrocytes compared with nontransplanted ones at 35–47 DPT and 110–130 DPT. However, this expression was normalized by 368–570 DPT. The upregulation of EAAT1/GLAST was uncoupled from EAAT2/GLT1 expression, with EAAT2/GLT1 showing similar expression between transplanted and nontransplanted astrocytes by 35–47 DPT. EAAT1/GLAST expression may take additional time to normalize in transplanted astrocytes. This is consistent with the finding that EAAT1/GLAST expression reaches significant levels earlier than EAAT2/GLT1 expression during astrocyte development in the brain and has differential regulation (Ullensvang et al., 1997; Todd and Hardingham, 2020). We also found lower expression of AQP4 at endfeet in transplanted astrocytes when compared with nontransplanted astrocytes at 35–47 DPT. However, AQP4 expression normalized in

transplanted astrocytes by 110–130 DPT. This is consistent with the known progressive increase in AQP4 at endfeet during postnatal mouse cortical development (Lunde et al., 2015). However, it remains to be determined whether the lower levels of AQP4 at endfeet of transplanted astrocytes are due to a general delay in maturation that affects AQP4 or a specific alteration (such as the contact between astrocytes and endothelial cells) that limits AQP4 enrichment at endfeet (Camassa et al., 2015). It should be noted that the astrocyte cultures used in this study do not contain endothelial cells. Thus, astrocytes only make contact with endothelial cells following their transplantation. It is possible that at 35–47 DPT, the developmental program of transplanted astrocytes is delayed, and they require additional time and cues from the local microenvironment to localize AQP4 at endfeet.

Another interesting finding is that astrocytes transplanted into the developing brain resemble neighboring nontransplanted astrocytes and do not show properties of reactivity. Several lines of evidence suggest that transplanted astrocytes develop appropriately in cortex and display hallmarks of healthy, nonreactive astrocytes: (1) they have low levels of GFAP, similar to neighboring nontransplanted astrocytes, (2) they have an elaborate

protoplasmic morphology and maintain their tiling behavior, (3) support synapses, (4) express similar amounts of EAAT2/GLT1 that is known to be downregulated in reactive astrocytes in neurologic diseases (Peterson and Binder, 2019), and (5) have normal calcium events. We do find, however, that when astrocytes are transplanted into the cortex of young adult mice, they are largely confined to the injection site, express high levels of GFAP, and display morphologic properties of reactive astrocytes. Why is the mature cortical environment less permissive to astrocyte integration? Several reasons may account for this: (1) transplanted astrocytes may not have sufficient space to grow/migrate in the more mature and densely packed parenchyma, (2) the extracellular environment may be less permissive to astrocyte elaboration and lack instructive factors that promote growth, (3) the transplantation process itself causes mechanical injury to mature brain tissue which is associated with pathologic processes (i.e., neuroinflammation) that interfere with proper astrocyte integration/maturation, hence promoting astrocyte reactivity. Future experiments will tackle these various issues to determine whether astrocyte integration can be improved in the mature brain, for example, by digesting chondroitin sulfate proteoglycans which may inhibit astrocyte migration and growth (Milbreta et al., 2014; Warren et al., 2020). Alternatively, inactivation of specific signaling pathways in transplanted astrocytes (i.e., STAT3) may also facilitate astrocyte integration and development by preventing reactivity and glial scar formation (Wanner et al., 2013).

Astrocyte transplantation may have a variety of useful applications for understanding the properties and functions of astrocytes and for intervening in CNS disorders and diseases. Given the ability of cortical astrocytes to integrate into the developing cortex, astrocyte transplantation could be used to assess astrocytic functions in neurodevelopmental disorders (NDDs). Astrocytic dysfunction has been associated with several NDDs, including autism spectrum disorders (Petrelli et al., 2016), Down syndrome (DS; Ponroy Bally and Murai, 2021), Fragile X (Jacobs and Doering, 2010), Rett syndrome (Jin et al., 2017), and schizophrenia (Dietz et al., 2020). Transplanting astrocytes obtained from NDD mouse models into wild-type mice may help characterize the specific impact of NDD-affected astrocytes on developing neural circuits in the brain. Indeed, studies have shown defects in astrocytic differentiation and maturation of transplanted schizophrenia-associated and Down syndrome-associated human iPSC-derived glia in the brains of immunodeficient mice (Chen et al., 2014; Windrem et al., 2017). It is also conceivable that early postnatal delivery of healthy astrocytes into NDD model mice through transplantation approaches may counteract alterations in brain development. Considering that excitatory/inhibitory (E/I) synaptic balance is affected in animal models of NDDs (Del Pino et al., 2018), astrocytes expressing exogenous glutamate/GABA biosensors (Marvin et al., 2018, 2019) or transporters may be a useful for monitoring and/or rebalancing extracellular levels of excitatory and inhibitory neurotransmitters in the brain.

Beyond NDDs, transplantation experiments into animal models of neurodegenerative diseases are likely to have important utility. Studies have shown the use of transplanted cells in reversing pathologic hallmarks associated to Alzheimer's (Pihlaja et al., 2008), Huntington's (Giralt et al., 2010), and Parkinson's disease (Proschel et al., 2014). In these studies, mouse astrocytes or human-derived astrocyte precursors injected into the adult rodent brain were found to exert a neuroprotective effect (Giralt et al.,

2010; Proschel et al., 2014) and contribute to β -amyloid plaque scavenging in Alzheimer's disease model mice (Pihlaja et al., 2008). However, the inefficient integration of transplanted astrocytes that we observed in the mature brain can potentially hinder the beneficial effect of this approach. Additional work is needed to improve integration of transplanted astrocytes to better understand the potential of astrocyte-based cell transplantation therapies in the mature CNS.

References

- Allen NJ, Eroglu C (2017) Cell biology of astrocyte-synapse interactions. *Neuron* 96:697–708.
- Bargaje R, Alam MP, Patowary A, Sarkar M, Ali T, Gupta S, Garg M, Singh M, Purkanti R, Scaria V, Sivasubbu S, Brahmachari V, Pillai B (2012) Proximity of H2A.Z containing nucleosome to the transcription start site influences gene expression levels in the mammalian liver and brain. *Nucleic Acids Res* 40:8965–8978.
- Batiuk MY, Martirosyan A, Wahis J, de Vin F, Marneffe C, Kusserow C, Koeppen J, Viana JF, Oliveira JF, Voet T, Ponting CP, Belgard TG, Holt MG (2020) Identification of region-specific astrocyte subtypes at single cell resolution. *Nat Commun* 11:1220.
- Bayraktar OA, et al. (2020) Astrocyte layers in the mammalian cerebral cortex revealed by a single-cell in situ transcriptomic map. *Nat Neurosci* 23:500–509.
- Ben Haim L, Rowitch DH (2017) Functional diversity of astrocytes in neural circuit regulation. *Nat Rev Neurosci* 18:31–41.
- Ben Menachem-Zidon O, Avital A, Ben-Menahem Y, Goshen I, Kreisel T, Shmueli EM, Segal M, Ben Hur T, Yirmiya R (2011) Astrocytes support hippocampal-dependent memory and long-term potentiation via interleukin-1 signaling. *Brain Behav Immun* 25:1008–1016.
- Boisvert MM, Erikson GA, Shokhirev MN, Allen NJ (2018) The aging astrocyte transcriptome from multiple regions of the mouse brain. *Cell Rep* 22:269–285.
- Bushong EA, Martone ME, Ellisman MH (2004) Maturation of astrocyte morphology and the establishment of astrocyte domains during postnatal hippocampal development. *Int J Dev Neurosci* 22:73–86.
- Cahoy JD, Emery B, Kaushal A, Foo LC, Zamanian JL, Christopherson KS, Xing Y, Lubischer JL, Krieg PA, Krupenko SA, Thompson WJ, Barres BA (2008) A transcriptome database for astrocytes, neurons, and oligodendrocytes: a new resource for understanding brain development and function. *J Neurosci* 28:264–278.
- Camassa LMA, Lunde LK, Hoddevik EH, Stensland M, Boldt HB, De Souza GA, Ottersen OP, Amiry-Moghaddam M (2015) Mechanisms underlying AQP4 accumulation in astrocyte endfeet. *Glia* 63:2073–2091.
- Chen C, Jiang P, Xue H, Peterson SE, Tran HT, McCann AE, Parast MM, Li S, Pleasure DE, Laurent LC, Loring JF, Liu Y, Deng W (2014) Role of astroglia in Down's syndrome revealed by patient-derived human-induced pluripotent stem cells. *Nat Commun* 5:4430.
- Chouchane M, Costa MR (2018) Culture and nucleofection of postnatal day 7 cortical and cerebellar mouse astroglial cells. *Bio Protoc* 8:e2712.
- Chow BW, Gu C (2015) The molecular constituents of the blood-brain barrier. *Trends Neurosci* 38:598–608.
- Clasadonte J, Scemes E, Wang Z, Boison D, Haydon PG (2017) Connexin 43-mediated astroglial metabolic networks contribute to the regulation of the sleep-wake cycle. *Neuron* 95:1365–1380.e5. e1365.
- Clavreul S, Abdeladim L, Hernandez-Garzon E, Niculescu D, Durand J, Ieng SH, Barry R, Bonvento G, Beaufrepaire E, Livet J, Loulier K (2019) Cortical astrocytes develop in a plastic manner at both clonal and cellular levels. *Nat Commun* 10:4884.
- Cohen-Salmon M, Slaoui L, Mazare N, Gilbert A, Oudart M, Alvear-Perez R, Elorza-Vidal X, Chever O, Boulay AC (2021) Astrocytes in the regulation of cerebrovascular functions. *Glia* 69:817–841.
- Coyne TM, Marcus AJ, Woodbury D, Black IB (2006) Marrow stromal cells transplanted to the adult brain are rejected by an inflammatory response and transfer donor labels to non-transplanted neurons and glia. *Stem Cells* 24:2483–2492.
- Del Pino I, Rico B, Marín O (2018) Neural circuit dysfunction in mouse models of neurodevelopmental disorders. *Curr Opin Neurobiol* 48:174–182.

- Dietz AG, Goldman SA, Nedergaard M (2020) Glial cells in schizophrenia: a unified hypothesis. *Lancet Psychiatry* 7:272–281.
- Emmett CJ, Lawrence JM, Raisman G, Seeley PJ (1991) Cultured epithelioid astrocytes migrate after transplantation into the adult rat brain. *J Comp Neurol* 311:330–341.
- Escartin C, et al. (2021) Reactive astrocyte nomenclature, definitions, and future directions. *Nat Neurosci* 24:312–325.
- Ezan P, André P, Cisternino S, Saubaméa B, Boulay AC, Doutremer S, Thomas MA, Quenec'h du N, Giaume C, Cohen-Salmon M (2012) Deletion of astroglial connexins weakens the blood-brain barrier. *J Cereb Blood Flow Metab* 32:1457–1467.
- Farmer WT, Murai K (2017) Resolving astrocyte heterogeneity in the CNS. *Front Cell Neurosci* 11:300.
- Farmer WT, Abrahamsson T, Chierzi S, Lui C, Zaelzer C, Jones EV, Bally BP, Chen GG, Thérout JF, Peng J, Bourque CW, Charron F, Ernst C, Sjöström PJ, Murai KK (2016) Neurons diversify astrocytes in the adult brain through sonic hedgehog signaling. *Science* 351:849–854.
- Filous AR, Miller JH, Coulson-Thomas YM, Horn KP, Alilain WJ, Silver J (2010) Immature astrocytes promote CNS axonal regeneration when combined with chondroitinase ABC. *Dev Neurobiol* 70:826–841.
- Frantz GD, McConnell SK (1996) Restriction of late cerebral cortical progenitors to an upper-layer fate. *Neuron* 17:55–61.
- Ge WP, Miyawaki A, Gage FH, Jan YN, Jan LY (2012) Local generation of glia is a major astrocyte source in postnatal cortex. *Nature* 484:376–380.
- Giralto A, Friedman HC, Caneda-Ferrón B, Urbán N, Moreno E, Rubio N, Blanco J, Peterson A, Canals JM, Alberch J (2010) BDNF regulation under GFAP promoter provides engineered astrocytes as a new approach for long-term protection in Huntington's disease. *Gene Ther* 17:1294–1308.
- Gourine AV, Kasymov V, Marina N, Tang F, Figueiredo MF, Lane S, Teschemacher AG, Spyer KM, Deisseroth K, Kasparov S (2010) Astrocytes control breathing through pH-dependent release of ATP. *Science* 329:571–575.
- Hatton JD, Nguyen MH, U HS (1993) Differential migration of astrocytes grafted into the developing rat brain. *Glia* 9:113–119.
- Hochstim C, Deneen B, Lukaszewicz A, Zhou Q, Anderson DJ (2008) Identification of positionally distinct astrocyte subtypes whose identities are specified by a homeodomain code. *Cell* 133:510–522.
- Ishii S, Sasaki T, Mohammad S, Hwang H, Tomy E, Somaa F, Ishibashi N, Okano H, Rakic P, Hashimoto-Torii K, Torii M (2021) Primary cilia safeguard cortical neurons in neonatal mouse forebrain from environmental stress-induced dendritic degeneration. *Proc Natl Acad Sci USA* 118:e2012482118.
- Jacobs S, Doering LC (2010) Astrocytes prevent abnormal neuronal development in the fragile x mouse. *J Neurosci* 30:4508–4514.
- Jin XR, Chen XS, Xiao L (2017) MeCP2 deficiency in neuroglia: new progress in the pathogenesis of Rett syndrome. *Front Mol Neurosci* 10:316.
- Kacem K, Lacombe P, Seylaz J, Bonvento G (1998) Structural organization of the perivascular astrocyte endfeet and their relationship with the endothelial glucose transporter: a confocal microscopy study. *Glia* 23:1–10.
- Khakh BS, Deneen B (2019) The emerging nature of astrocyte diversity. *Annu Rev Neurosci* 42:187–207.
- Kim JG, Suyama S, Koch M, Jin S, Argente-Arizon P, Argente J, Liu ZW, Zimmer MR, Jeong JK, Szigeti-Buck K, Gao Y, Garcia-Caceres C, Yi CX, Salmaso N, Vaccarino FM, Chowen J, Diano S, Dietrich MO, Tschöp MH, Horvath TL (2014) Leptin signaling in astrocytes regulates hypothalamic neuronal circuits and feeding. *Nat Neurosci* 17:908–910.
- Kirdajova D, Valihrach L, Valny M, Kriska J, Krocianova D, Benesova S, Abaffy P, Zucha D, Klassen R, Kolenicova D, Honsa P, Kubista M, Anderova M (2021) Transient astrocyte-like NG2 glia subpopulation emerges solely following permanent brain ischemia. *Glia* 69:2658–2681.
- Kita Y, Kawakami K, Takahashi Y, Murakami F (2013) Development of cerebellar neurons and glia revealed by in utero electroporation: Golgi-like labeling of cerebellar neurons and glia. *PLoS One* 8:e70091.
- Lanjakornsiripan D, Pior BJ, Kawaguchi D, Furutachi S, Tahara T, Katsuyama Y, Suzuki Y, Fukazawa Y, Gotoh Y (2018) Layer-specific morphological and molecular differences in neocortical astrocytes and their dependence on neuronal layers. *Nat Commun* 9:1623.
- Lewis SA, Cowan NJ (1985) Temporal expression of mouse glial fibrillary acidic protein mRNA studied by a rapid in situ hybridization procedure. *J Neurochem* 45:913–919.
- Lordkipanidze T, Dunaevsky A (2005) Purkinje cell dendrites grow in alignment with Bergmann glia. *Glia* 51:229–234.
- Lunde LK, Camassa LM, Hoddevik EH, Khan FH, Ottersen OP, Boldt HB, Amiry-Moghaddam M (2015) Postnatal development of the molecular complex underlying astrocyte polarization. *Brain Struct Funct* 220:2087–2101.
- Madisen L, Zwingman TA, Sunkin SM, Oh SW, Zariwala HA, Gu H, Ng LL, Palmiter RD, Hawrylycz MJ, Jones AR, Lein ES, Zeng H (2010) A robust and high-throughput Cre reporting and characterization system for the whole mouse brain. *Nat Neurosci* 13:133–140.
- Marshall CA, Novitch BG, Goldman JE (2005) Olig2 directs astrocyte and oligodendrocyte formation in postnatal subventricular zone cells. *J Neurosci* 25:7289–7298.
- Marvin JS, et al. (2018) Stability, affinity, and chromatic variants of the glutamate sensor iGluSnFR. *Nat Methods* 15:936–939.
- Marvin JS, Shimoda Y, Magloire V, Leite M, Kawashima T, Jensen TP, Kolb I, Knott EL, Novak O, Podgorski K, Leidenheimer NJ, Rusakov DA, Ahrens MB, Kullmann DM, Looger LL (2019) A genetically encoded fluorescent sensor for in vivo imaging of GABA. *Nat Methods* 16:763–770.
- Mestre H, Mori Y, Nedergaard M (2020) The brain's glymphatic system: current controversies. *Trends Neurosci* 43:458–466.
- Milbreta U, von Boxberg Y, Maily P, Nothias F, Soares S (2014) Astrocytic and vascular remodeling in the injured adult rat spinal cord after chondroitinase ABC treatment. *J Neurotrauma* 31:803–818.
- Müller CM, Best J (1989) Ocular dominance plasticity in adult cat visual cortex after transplantation of cultured astrocytes. *Nature* 342:427–430.
- Ogata K, Kosaka T (2002) Structural and quantitative analysis of astrocytes in the mouse hippocampus. *Neuroscience* 113:221–233.
- Papadopoulos MC, Verkman AS (2013) Aquaporin water channels in the nervous system. *Nat Rev Neurosci* 14:265–277.
- Peterson AR, Binder DK (2019) Regulation of synaptosomal GLT-1 and GLAST during epileptogenesis. *Neuroscience* 411:185–201.
- Petrelli F, Pucci L, Bezzi P (2016) Astrocytes and microglia and their potential link with autism spectrum disorders. *Front Cell Neurosci* 10:21.
- Petzold GC, Albeanu DF, Sato TF, Murthy VN (2008) Coupling of neural activity to blood flow in olfactory glomeruli is mediated by astrocytic pathways. *Neuron* 58:897–910.
- Pihlaja R, Koistinaho J, Malm T, Sikkila H, Vainio S, Koistinaho M (2008) Transplanted astrocytes internalize deposited beta-amyloid peptides in a transgenic mouse model of Alzheimer's disease. *Glia* 56:154–163.
- Ponroy Bally B, Murai KK (2021) Astrocytes in Down syndrome across the lifespan. *Front Cell Neurosci* 15:702685.
- Proschel C, Stripay JL, Shih CH, Munger JC, Noble MD (2014) Delayed transplantation of precursor cell-derived astrocytes provides multiple benefits in a rat model of Parkinsons. *EMBO Mol Med* 6:504–518.
- Rash JE, Yasumura T, Dudek FE, Nagy JI (2001) Cell-specific expression of connexins and evidence of restricted gap junctional coupling between glial cells and between neurons. *J Neurosci* 21:1983–2000.
- Rege M, Subramanian V, Zhu C, Hsieh TH, Weiner A, Friedman N, Claudier-Münster S, Steinmetz LM, Rando OJ, Boyer LA, Peterson CL (2015) Chromatin dynamics and the RNA exosome function in concert to regulate transcriptional homeostasis. *Cell Rep* 13:1610–1622.
- Rose CR, Ziemens D, Untiet V, Fahlke C (2018) Molecular and cellular physiology of sodium-dependent glutamate transporters. *Brain Res Bull* 136:3–16.
- Saab AS, Neumeyer A, Jahn HM, Cupido A, Šimek AA, Boele HJ, Scheller A, Le Meur K, Götz M, Monyer H, Sprengel R, Rubio ME, Deitmer JW, De Zeeuw CI, Kirchhoff F (2012) Bergmann glial AMPA receptors are required for fine motor coordination. *Science* 337:749–753.
- Salmon CK, Syed TA, Kacerovsky JB, Alivodej N, Schober AL, Pratte MT, Rosen MP, Green M, DasGupta A, Vali H, Mandato CA, Siddiqi K, Murai KK (2021) Organizing principles of astrocytic nanoarchitecture in the mouse cerebral cortex. *bioRxiv* 467391. <https://doi.org/10.1101/2021.11.05.467391>.
- Sattler R, Rothstein JD (2006) Regulation and dysregulation of glutamate transporters. *Handb Exp Pharmacol* (175):277–303.
- Schummers J, Yu H, Sur M (2008) Tuned responses of astrocytes and their influence on hemodynamic signals in the visual cortex. *Science* 320:1638–1643.
- Smith GM, Miller RH (1991) Immature type-1 astrocytes suppress glial scar formation, are motile and interact with blood vessels. *Brain Res* 543:111–122.

- Sofroniew MV, Vinters HV (2010) Astrocytes: biology and pathology. *Acta Neuropathol* 119:7–35.
- Srinivasan R, Lu TY, Chai H, Xu J, Huang BS, Golshani P, Coppola G, Khakh BS (2016) New transgenic mouse lines for selectively targeting astrocytes and studying calcium signals in astrocyte processes in situ and in vivo. *Neuron* 92:1181–1195.
- Stackhouse TL, Mishra A (2021) Neurovascular coupling in development and disease: focus on astrocytes. *Front Cell Dev Biol* 9:702832.
- Stirling DR, Swain-Bowden MJ, Lucas AM, Carpenter AE, Cimini BA, Goodman A (2021) CellProfiler 4: improvements in speed, utility and usability. *BMC Bioinformatics* 22:433.
- Tan CX, Burrus Lane CJ, Eroglu C (2021) Role of astrocytes in synapse formation and maturation. *Curr Top Dev Biol* 142:371–407.
- Todd AC, Hardingham GE (2020) The regulation of astrocytic glutamate transporters in health and neurodegenerative diseases. *Int J Mol Sci* 21:9607.
- Tsai HH, Li H, Fuentealba LC, Molofsky AV, Taveira-Marques R, Zhuang H, Tenney A, Murnen AT, Fancy SP, Merkle F, Kessaris N, Alvarez-Buylla A, Richardson WD, Rowitch DH (2012) Regional astrocyte allocation regulates CNS synaptogenesis and repair. *Science* 337:358–362.
- Ullensvang K, Lehre KP, Storm-Mathisen J, Danbolt NC (1997) Differential developmental expression of the two rat brain glutamate transporter proteins GLAST and GLT. *Eur J Neurosci* 9:1646–1655.
- Wakida NM, Cruz GMS, Ro CC, Moncada EG, Khatibzadeh N, Flanagan LA, Berns MW (2018) Phagocytic response of astrocytes to damaged neighboring cells. *PLoS One* 13:e0196153.
- Wang Y, DelRosso NV, Vaidyanathan TV, Cahill MK, Reitman ME, Pittolo S, Mi X, Yu G, Poskanzer KE (2019) Accurate quantification of astrocyte and neurotransmitter fluorescence dynamics for single-cell and population-level physiology. *Nat Neurosci* 22:1936–1944.
- Wanner IB, Anderson MA, Song B, Levine J, Fernandez A, Gray-Thompson Z, Ao Y, Sofroniew MV (2013) Glial scar borders are formed by newly proliferated, elongated astrocytes that interact to corral inflammatory and fibrotic cells via STAT3-dependent mechanisms after spinal cord injury. *J Neurosci* 33:12870–12886.
- Warren PM, Andrews MR, Smith M, Bartus K, Bradbury EJ, Verhaagen J, Fawcett JW, Kwok JCF (2020) Secretion of a mammalian chondroitinase ABC aids glial integration at PNS/CNS boundaries. *Sci Rep* 10:11262.
- Welle A, Kasakow CV, Jungmann AM, Gobbo D, Stopper L, Nordstrom K, Salhab A, Gasparoni G, Scheller A, Kirchhoff F, Walter J (2021) Epigenetic control of region-specific transcriptional programs in mouse cerebellar and cortical astrocytes. *Glia* 69:2160–2177.
- Windrem MS, Osipovitch M, Liu Z, Bates J, Chandler-Militello D, Zou L, Munir J, Schanz S, McCoy K, Miller RH, Wang S, Nedergaard M, Findling RL, Tesar PJ, Goldman SA (2017) Human iPSC glial mouse chimeras reveal glial contributions to schizophrenia. *Cell Stem Cell* 21:195–208.e6. e196.
- Yamada K, Watanabe M (2002) Cytodifferentiation of Bergmann glia and its relationship with Purkinje cells. *Anat Sci Int* 77:94–108.
- Zhang K, Chen C, Yang Z, He W, Liao X, Ma Q, Deng P, Lu J, Li J, Wang M, Li M, Zheng L, Zhou Z, Sun W, Wang L, Jia H, Yu Z, Zhou Z, Chen X (2016) Sensory response of transplanted astrocytes in adult mammalian cortex in vivo. *Cereb Cortex* 26:3690–3704.
- Zhang Y, Sloan SA, Clarke LE, Caneda C, Plaza CA, Blumenthal PD, Vogel H, Steinberg GK, Edwards MS, Li G, Duncan JA 3rd, Cheshier SH, Shuer LM, Chang EF, Grant GA, Gephart MG, Barres BA (2016) Purification and characterization of progenitor and mature human astrocytes reveals transcriptional and functional differences with mouse. *Neuron* 89:37–53.
- Zhou HF, Lund RD (1992) Migration of astrocytes transplanted to the mid-brain of neonatal rats. *J Comp Neurol* 317:145–155.
- Zhu X, Zuo H, Maher BJ, Serwanski DR, LoTurco JJ, Lu QR, Nishiyama A (2012) Olig2-dependent developmental fate switch of NG2 cells. *Development* 139:2299–2307.
- Zuo H, Wood WM, Sherfat A, Hill RA, Lu QR, Nishiyama A (2018) Age-dependent decline in fate switch from NG2 cells to astrocytes after Olig2 deletion. *J Neurosci* 38:2359–2371.